Supplementary Information for:

Crystal chemistry and thermodynamics of HREE (Er, Yb) mixing in xenotime solid solution

Andrew C. Strzelecki[1,2,3,4], Margaret Reece[1,2], Xiaodong Zhao[1,2], Wendy Yu[1,2], Chris Benmore[5], Yang Ren[5,6], Christopher Alcorn[4], Artaches Migdisov[4], Hongwu Xu[4,7], Xiaofeng Guo[1,2,3,*]

[1] *Department of Chemistry, Washington State University, Pullman, Washington 99164, United States*

[2] *Alexandra Navrotsky Institute for Experimental Thermodynamics, Washington State University, Pullman, Washington 99164, United States*

[3] *Materials Science and Engineering, Washington State University, Pullman, Washington 99164, United States*

[4] *Earth and Environmental Sciences Division, Los Alamos National Laboratory, Los Alamos, New Mexico 87545, United States*

[5] *X-ray Science Division, Argonne National Laboratory, 9700 South Cass Avenue, Argonne, Illinois, 60439, United States*

[6] *Department of Physics, City University of Hong Kong, Kowloon Hong Kong, China*

[7] *School of Molecular Sciences, Center for Materials of the Universe, Arizona State University, Tempe, Arizona 85287, United States*

---

* e-mail: x.guo@wsu.edu

S1: Supplementary Figures and Tables Referred to in the Main Text:

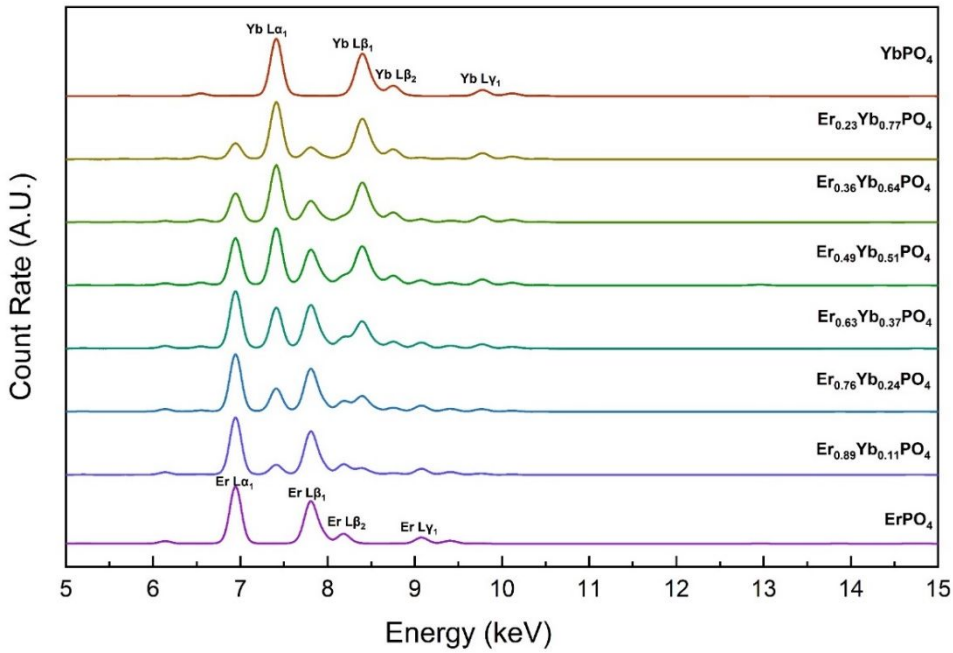

Figure S1 XRF spectra collected for the first batch of $Er_{(x)}Yb_{(1-x)}PO_4$

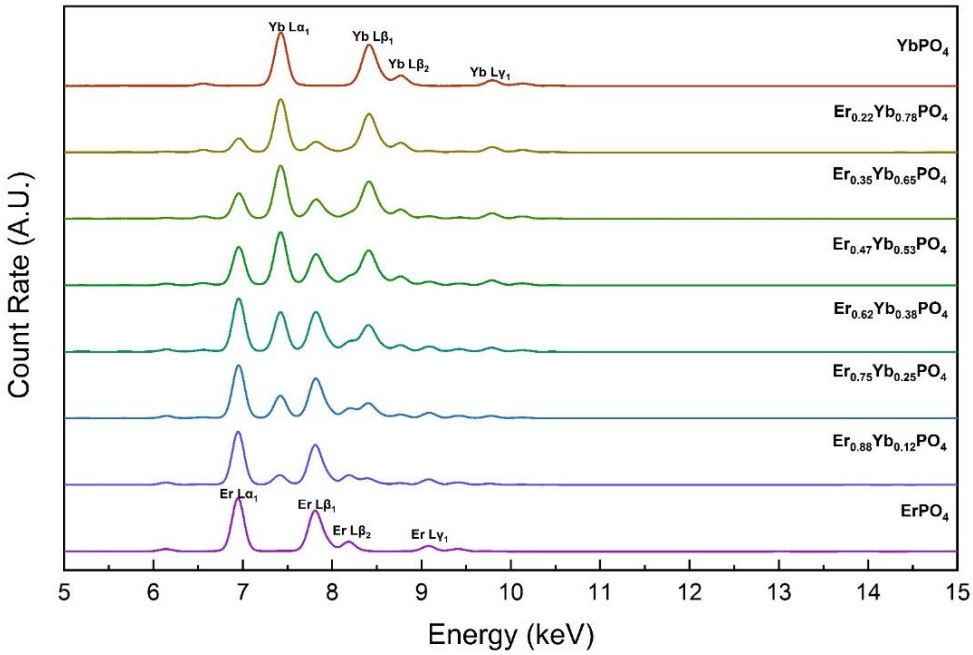

Figure S2 XRF spectra collected for the second batch of $Er_{(x)}Yb_{(1-x)}PO_4$

Table S1 Atoms per formula units for Er and Yb, as determine by XRF for the pristine $Er_{(x)}Yb_{(1-x)}PO_4$ samples.

Empirical Formula	Er (apfu)	Yb (apfu)
$ErPO_4$	1.0000	0.0000
$ErPO_4$	1.0000	0.0000
$Er_{0.89}Yb_{0.11}PO_4$	0.88585 ± 0.00004	0.11415 ± 0.00004
$Er_{0.88}Yb_{0.12}PO_4$	0.8787 ± 0.0001	0.1213 ± 0.0001
$Er_{0.76}Yb_{0.24}PO_4$	0.7576 ± 0.0002	0.2424 ± 0.0002
$Er_{0.75}Yb_{0.25}PO_4$	0.7465 ± 0.0001	0.2535 ± 0.0001
$Er_{0.63}Yb_{0.37}PO_4$	0.6343 ± 0.0002	0.3657 ± 0.0002
$Er_{0.62}Yb_{0.38}PO_4$	0.6175 ± 0.0001	0.3825 ± 0.0001
$Er_{0.49}Yb_{0.51}PO_4$	0.4945 ± 0.0001	0.5055 ± 0.0001
$Er_{0.47}Yb_{0.53}PO_4$	0.4693 ± 0.0004	0.5307 ± 0.0004
$Er_{0.36}Yb_{0.64}PO_4$	0.3640 ± 0.0001	0.6360 ± 0.0001
$Er_{0.35}Yb_{0.65}PO_4$	0.3507 ± 0.0002	0.6493 ± 0.0002
$Er_{0.23}Yb_{0.77}PO_4$	0.2340 ± 0.0002	0.7660 ± 0.0002
$Er_{0.22}Yb_{0.78}PO_4$	0.2208 ± 0.0002	0.7792 ± 0.0002
$YbPO_4$	0.0000	1.0000

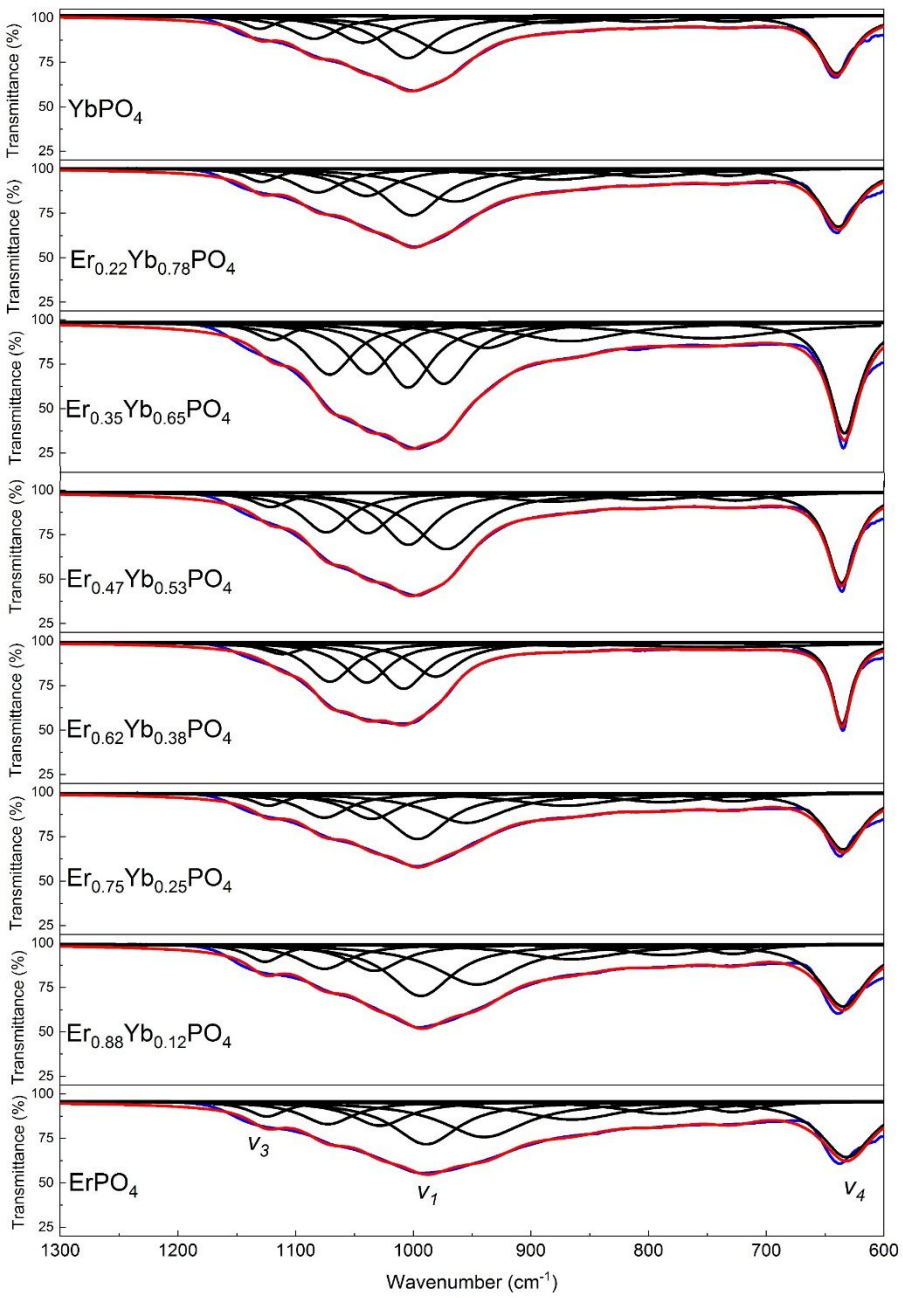

Figure S3 FTIR spectra recorded in the 600 – 1300 cm^{-1} range for pristine $Er_{(x)}Yb_{(1-x)}PO_4$. The *blue* curve indicates the data, and the *red* curve indicates the fitting.

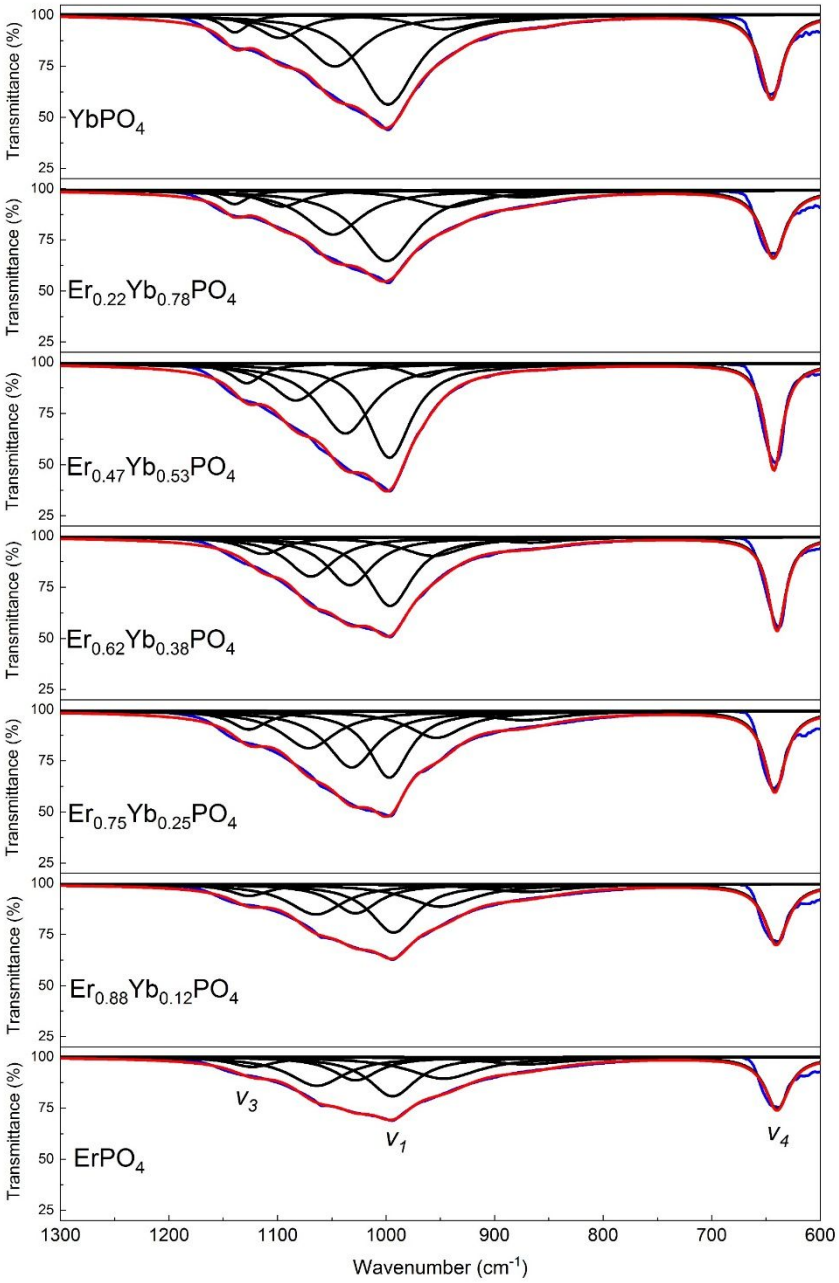

Figure S4 FTIR spectra recorded in the 600 – 1300 cm^{-1} range for the $Er_{(x)}Yb_{(1-x)}PO_4$ recovered after the TGA-DSC experiments to 1200°C. The *blue* curve indicates the data, and the *red* curve indicates the fitting.

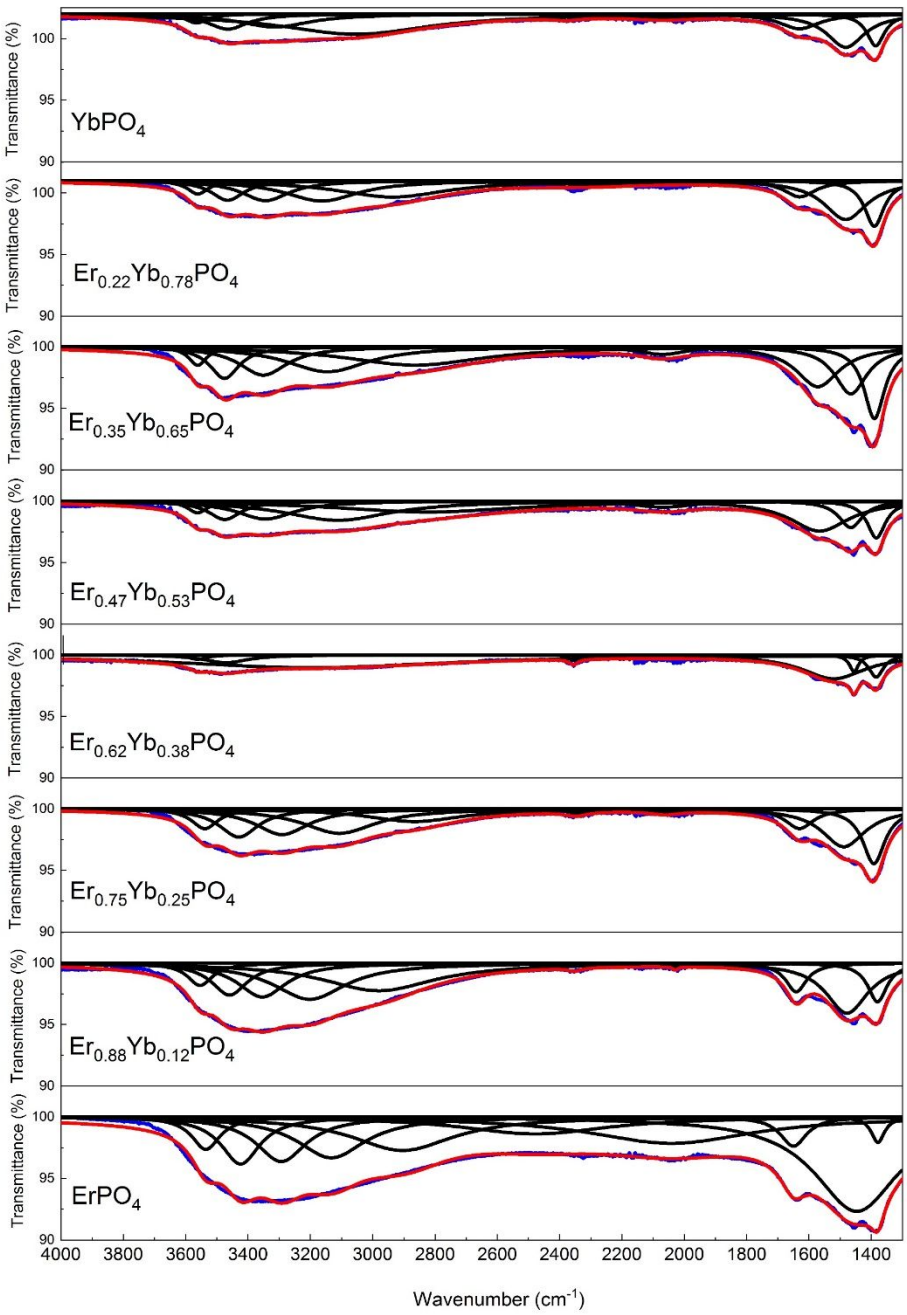

Figure S5 FTIR spectra recorded in the 1300 – 4000 cm^{-1} range for pristine $Er_{(x)}Yb_{(1-x)}PO_4$. The *blue* curve indicates the data, and the *red* curve indicates the fitting.

Table S2 Location of the internal vibrational modes (cm^{-1}) of PO_4 in batch #2 of the pristine $Er_{(x)}Yb_{(1-x)}PO_4$, as determined by deconvolution via a Lorentz function.

Sample	$\nu_{as}(PO_4)$			$\nu_s(PO_4)$			$\delta_{as}(PO_4)$
$ErPO_4$	1124.3	1072.5	1028.3	988.9	939.6	865.0	631.7
error	0.8	1.6	2.5	1.8	2.9	3.6	0.2
$Er_{0.88}Yb_{0.22}PO_4$	1125.9	1075.5	1032.7	993.5	946.0	865.7	634.7
error	0.7	1.6	2.3	1.5	3.0	4.2	0.2
$Er_{0.75}Yb_{0.25}PO_4$	1122.9	1075.6	1035.1	996.3	954.6	871.5	634.7
error	0.9	1.4	1.9	1.3	4.0	3.6	0.1
$Er_{0.62}Yb_{0.38}PO_4$	1111.0	1070.7	1039.6	1008.2	981.0	866.0	635.7
error	1.3	1.1	1.2	1.0	1.9	4.3	0.1
$Er_{0.47}Yb_{0.53}PO_4$	1121.1	1074.0	1038.7	1004.2	971.9	882.0	636.1
error	1.0	1.3	1.4	1.3	2.4	4.6	0.1
$Er_{0.35}Yb_{0.65}PO_4$	1119.1	1070.9	1037.6	1004.4	974.2	937.7	633.5
error	1.0	1.5	1.6	1.6	2.0	5.8	0.1
$Er_{0.22}Yb_{0.78}PO_4$	1128.7	1081.1	1039.8	1001.0	964.5	880.1	638.6
error	0.8	1.4	1.9	1.4	4.6	4.9	0.1
$YbPO_4$	1130.5	1084.0	1042.9	1004.6	970.6	881.6	640.4
error	0.7	1.3	1.7	1.3	3.3	6.5	0.1

Table S3 Location of the normal vibrational modes (cm^{-1}) of H_2O, OH, and CO_2 in batch #2 of the pristine $Er_{(x)}Yb_{(1-x)}PO_4$, as determined by deconvolution via a Lorentz function.

Sample	$\delta(OH)$	$\nu_s(CO_2)$	$\delta(H_2O)$	$\nu_{as}(CO_2)$		$\nu(OH)$			ν_s (H_2O)	ν_{as} (H_2O)
$ErPO_4$	1378.8	1446.8	1649.8	2041.5	2478.1	2904.1	3133.0	3293.4	3424.0	3535.1
error	0.5	1.0	0.6	7.1	8.1	5.6	3.4	2.0	1.2	1.1
$Er_{0.88}Yb_{0.22}PO_4$	1380.4	1478.1	1641.1	2028.6	2351.8	2980.3	3202.2	3354.3	3459.5	3553.8
error	0.3	0.7	0.3	1.3	2.2	4.9	3.9	2.7	1.6	1.1
$Er_{0.75}Yb_{0.25}PO_4$	1391.9	1488.5	1630.5	2062.1	2348.1	2865.6	3107.2	3290.8	3429.7	3538.6
error	0.3	1.0	0.8	3.0	2.1	5.8	2.9	2.0	1.1	1.0
$Er_{0.62}Yb_{0.38}PO_4$	1384.6	1455.4	1520.8	-	2355.5	-	3190.0	-	3470.2	3561.5
error	0.2	0.2	1.2	-	0.6	-	3.3	-	2.8	1.5
$Er_{0.47}Yb_{0.53}PO_4$	1383.9	1465.8	1566.1	2067.2	-	2820.9	3112.4	3344.0	3474.5	3562.1
error	0.2	0.4	1.4	1.8	-	18.6	3.6	2.4	1.0	0.9
$Er_{0.35}Yb_{0.65}PO_4$	1390.2	1465.8	1571.6	2070.1	-	2863.6	3145.1	3350.9	3475.2	3561.2
error	0.4	1.0	1.6	2.1	-	7.9	2.9	1.7	0.8	0.9
$Er_{0.22}Yb_{0.78}PO_4$	1390.4	1482.2	1629.4	-	2317.4	2936.1	3163.6	3343.9	3465.1	3560.9
error	0.2	0.9	0.9	-	7.8	7.2	2.9	2.0	1.2	1.0
$YbPO_4$	1386.1	1482.0	1630.3	2065.5	2379.2	-	3053.7	3315.4	3464.9	3565.1
error	0.2	0.4	0.9	2.6	2.4	-	4.0	3.6	1.1	0.9

Table S4 Location of the internal vibration modes of PO_4 in batch #2 of $Er_{(x)}Yb_{(1-x)}PO_4$ after TGA-DSC to 1200°C, as determined by deconvolution via a Lorentz function.

Sample	$\nu_{as}(PO_4)$			$\nu_s(PO_4)$			$\delta_{as}(PO_4)$
$ErPO_4$	1123.2	1063.6	1028.2	994.1	946.8	871.2	639.8
error	1.7	2.9	2.1	1.5	3.2	4.7	0.1
$Er_{0.88}Yb_{0.22}PO_4$	1126.1	1064.4	1028.2	993.1	949.6	870.1	640.6
error	1.3	2.9	1.9	1.2	3.7	4.7	0.1
$Er_{0.75}Yb_{0.25}PO_4$	1126.2	1071.1	1031.7	997.1	953.7	872.9	641.9
error	1.1	2.6	1.3	0.8	2.1	3.6	0.1
$Er_{0.62}Yb_{0.38}PO_4$	1113.0	1069.1	1033.3	996.2	957.3	866.9	639.8
error	1.4	1.5	1.1	0.7	4.1	3.5	0.1
$Er_{0.47}Yb_{0.53}PO_4$	1128.4	1083.0	1037.5	996.9	965.6	854.8	642.7
error	0.8	1.3	0.9	0.6	3.7	5.8	0.1
$Er_{0.35}Yb_{0.65}PO_4$	-	-	-	-	-	-	-
error	-	-	-	-	-	-	-
$Er_{0.22}Yb_{0.78}PO_4$	1139.6	1096.0	1048.9	999.5	942.5	874.8	643.3
error	0.8	1.8	1.1	0.7	2.8	4.4	0.1
$YbPO_4$	1139.2	1097.8	1047.1	998.3	945.7	864.0	645.0
error	0.8	1.3	1.0	0.6	4.2	4.4	0.1

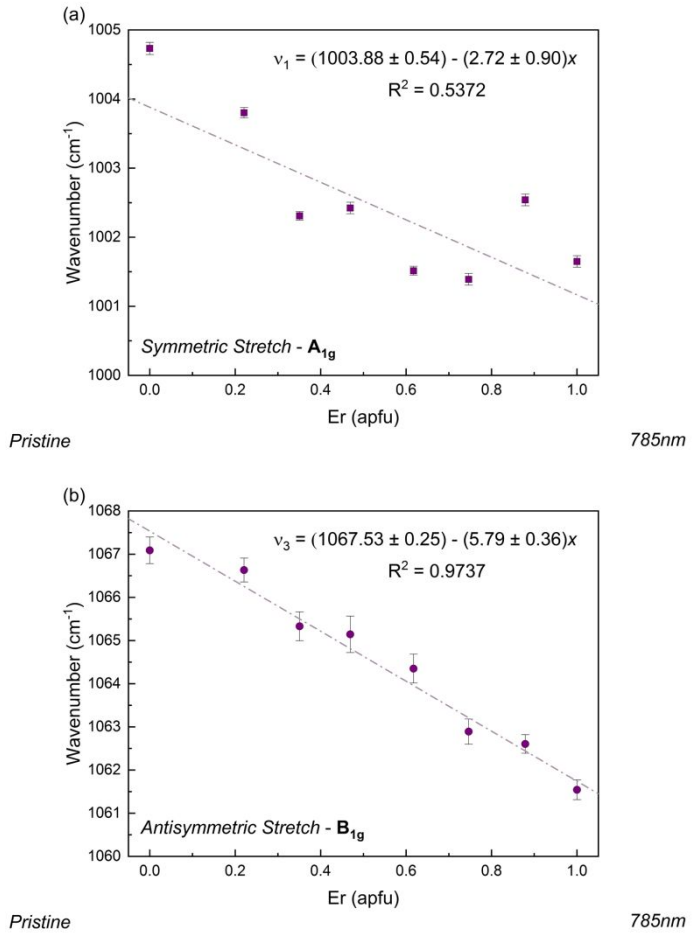

Figure S6 Variation in the P-O Raman stretching modes in pristine $Er_{(x)}Yb_{(1-x)}PO_4$ as a function of *x*.

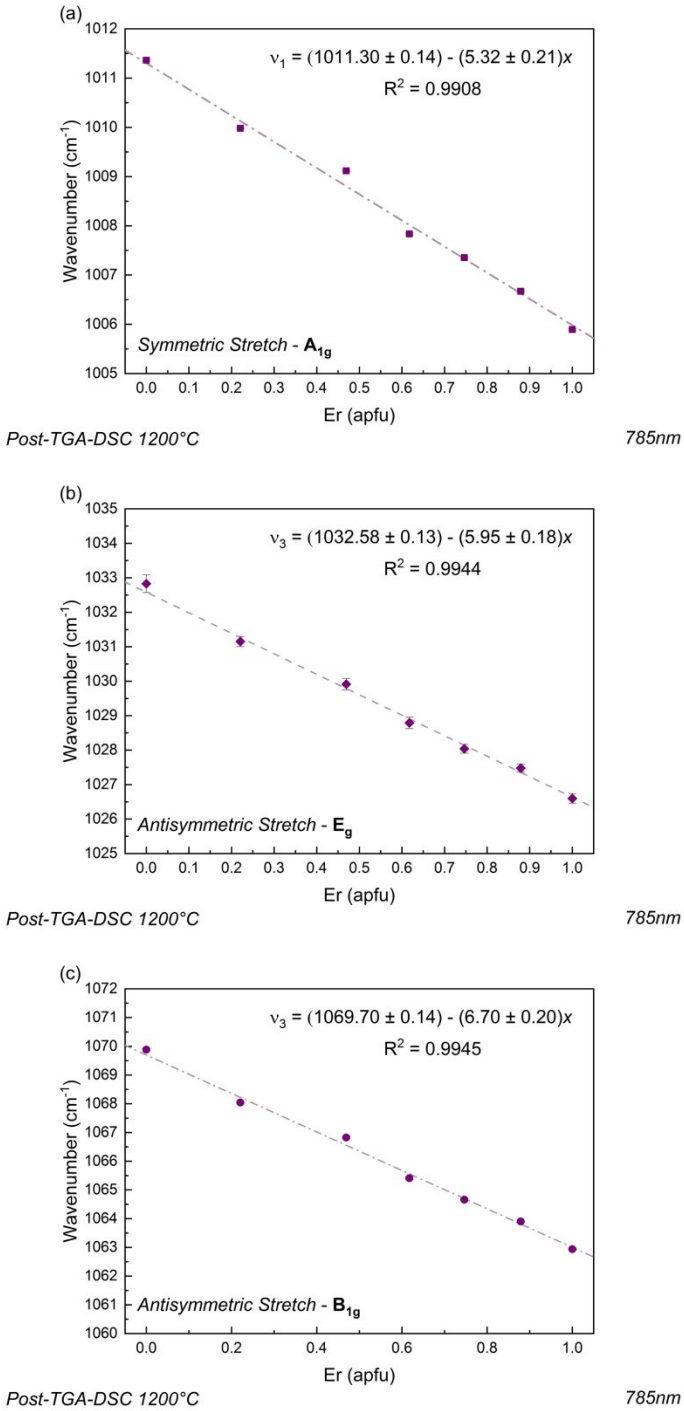

Figure S7 Variation in the P-O Raman stretching modes in the recovered $Er_{(x)}Yb_{(1-x)}PO_4$ post TGA-DSC to 1200°C as a function of *x*.

Table S5 Location of the internal vibrational modes (cm^{-1}) of PO_4 in batch #2 of the pristine $Er_{(x)}Yb_{(1-x)}PO_4$, as determined by deconvolution via a Lorentz function.

Er (x) [apfu]			v_1 (A_{1g}) [cm^{-1}]			v_3 (B_{2g}) [cm^{-1}]			adj. R^2
1.0000	±	0.0000	1001.65	±	0.08	1061.54	±	0.23	0.972
0.8787	±	0.0001	1002.54	±	0.08	1062.60	±	0.22	0.969
0.7465	±	0.0001	1001.39	±	0.08	1062.89	±	0.29	0.973
0.6175	±	0.0001	1001.51	±	0.06	1064.35	±	0.33	0.981
0.4693	±	0.0004	1002.42	±	0.08	1065.14	±	0.42	0.967
0.3507	±	0.0002	1002.31	±	0.06	1065.33	±	0.33	0.983
0.2208	±	0.0002	1003.80	±	0.07	1066.63	±	0.28	0.975
0.0000	±	0.0000	1004.73	±	0.09	1067.09	±	0.31	0.977

Table S6 Location of the internal vibration modes of PO_4 in batch #2 of $Er_{(x)}Yb_{(1-x)}PO_4$ after TGA-DSC to 1200°C, as determined by deconvolution via a Lorentz function.

Er (x) [apfu]			v_1 (A_{1g}) [cm^{-1}]			v_3 (B_{2g}) [cm^{-1}]			v_3 (E_g) [cm^{-1}]			adj. R^2
1.0000	±	0.0000	1005.89	±	0.02	1062.94	±	0.03	1026.60	±	0.14	0.989
0.8787	±	0.0001	1006.67	±	0.02	1063.90	±	0.03	1027.48	±	0.11	0.993
0.7465	±	0.0001	1007.35	±	0.02	1064.66	±	0.03	1028.04	±	0.13	0.991
0.6175	±	0.0001	1007.83	±	0.02	1065.41	±	0.05	1028.79	±	0.17	0.989
0.4693	±	0.0004	1009.12	±	0.02	1066.82	±	0.04	1029.92	±	0.17	0.991
0.2208	±	0.0002	1009.98	±	0.01	1068.04	±	0.03	1031.15	±	0.15	0.995
0.0000	±	0.0000	1011.36	±	0.02	1069.88	±	0.05	1032.83	±	0.26	0.988

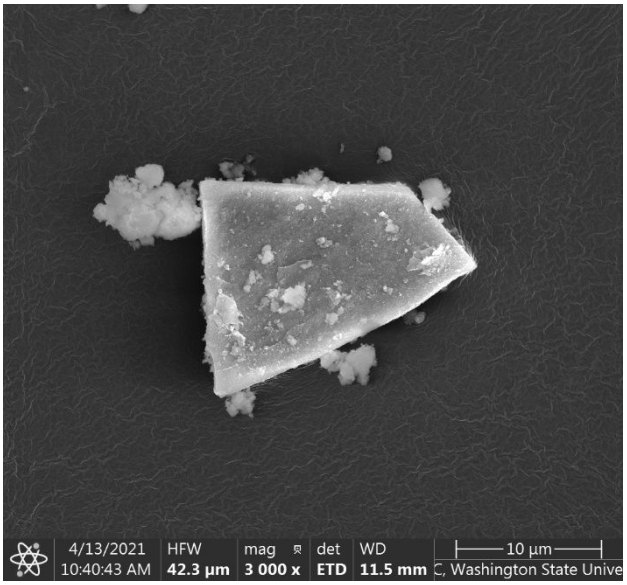

Figure S8 SEM image of Pristine $ErPO_4$

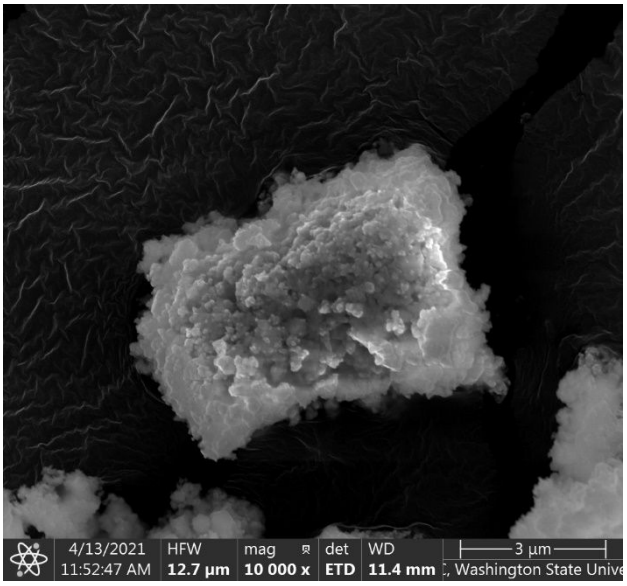

Figure S9 SEM image of $ErPO_4$ recovered after TGA-DSC to 1200°C.

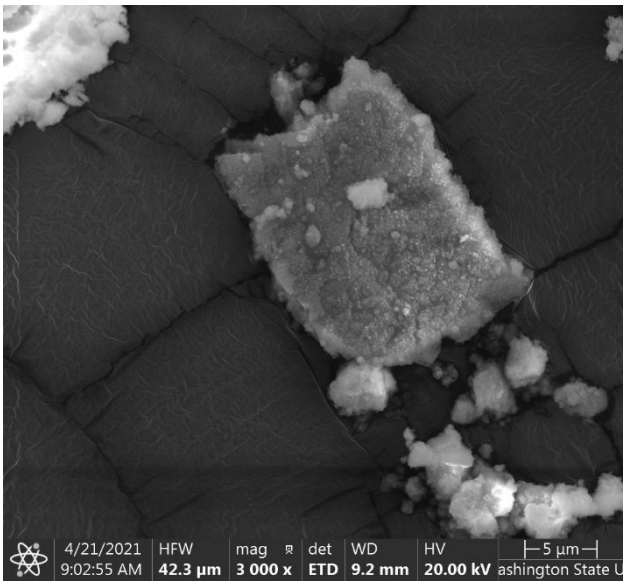

Figure S10 SEM image of Pristine $Er_{0.75}Yb_{0.25}PO_4$

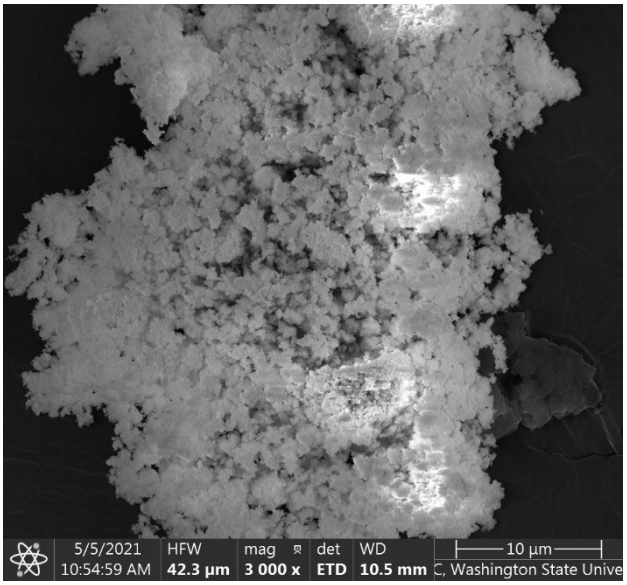

Figure S11 SEM image of $Er_{0.75}Yb_{0.25}PO_4$ recovered after TGA-DSC to 1200°C.

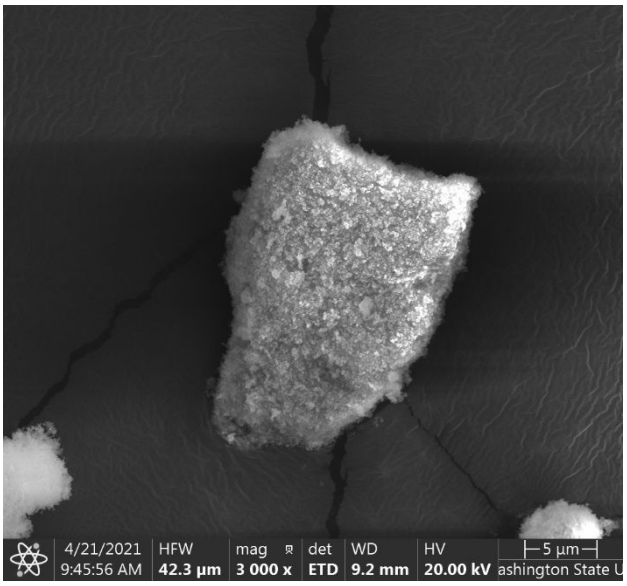

Figure S12 SEM image of Pristine $Er_{0.47}Yb_{0.53}PO_4$

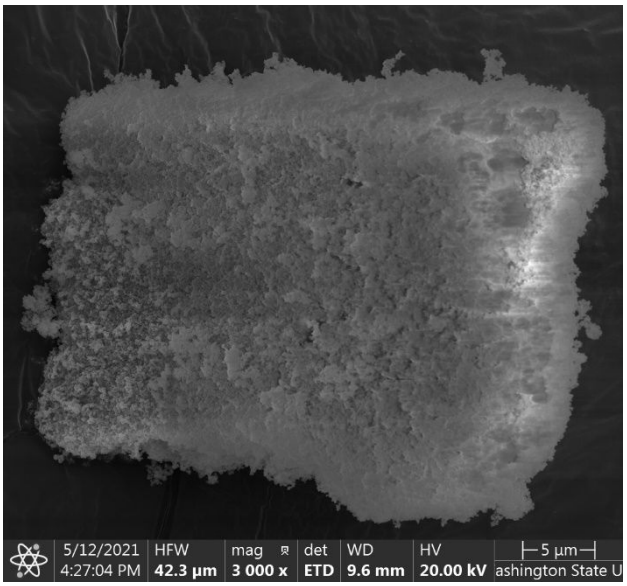

Figure S13 SEM image of $Er_{0.47}Yb_{0.53}PO_4$ recovered after TGA-DSC to 1200°C.

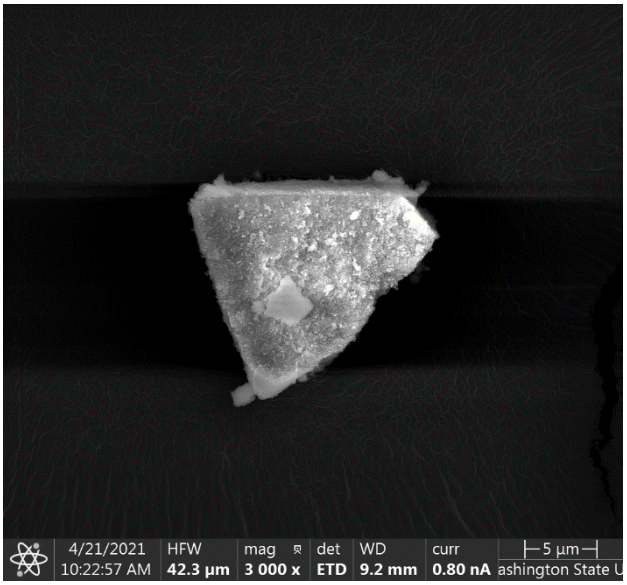

Figure S14 SEM image of Pristine $Er_{0.22}Yb_{0.78}PO_4$

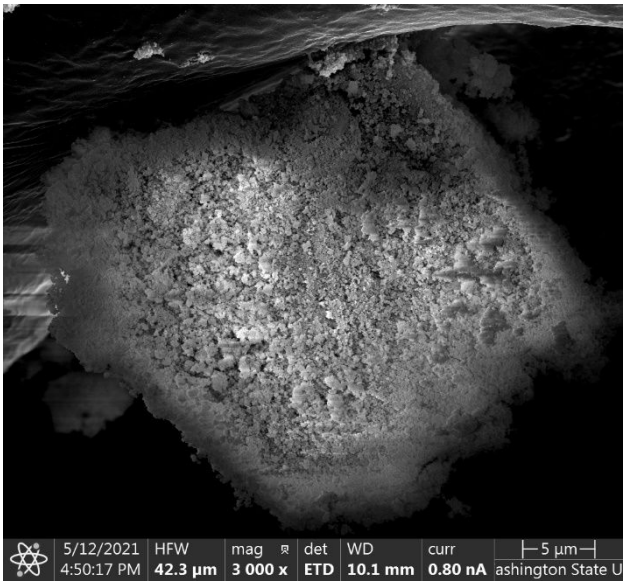

Figure S15 SEM image of $Er_{0.22}Yb_{0.78}PO_4$ recovered after TGA-DSC to 1200°C.

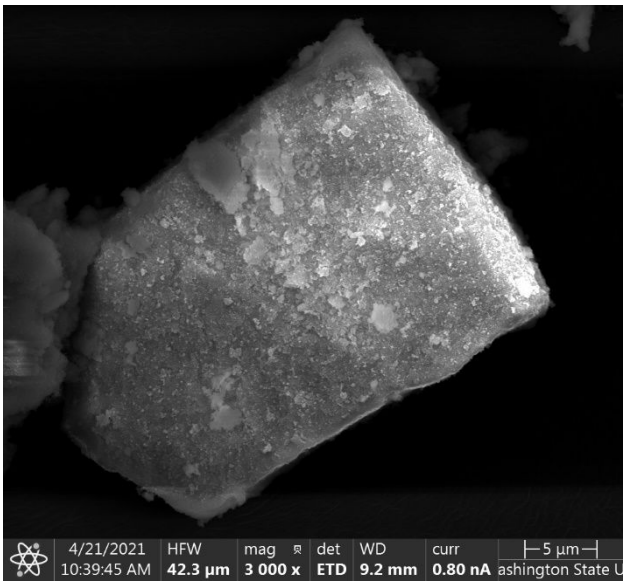

Figure S16 SEM image of Pristine $YbPO_4$

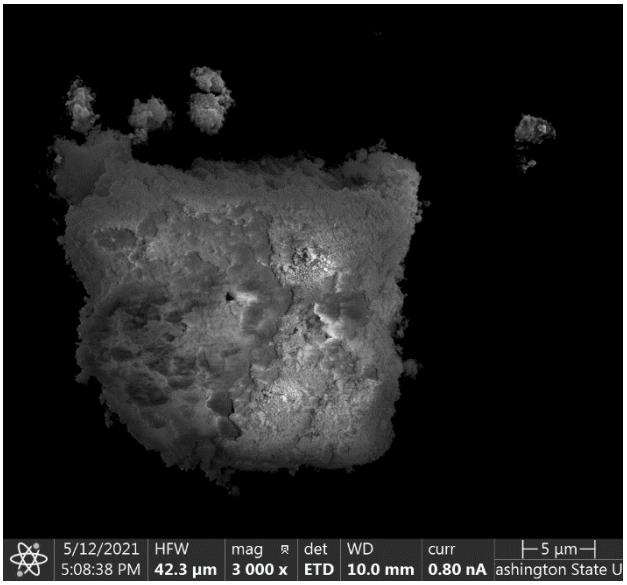

Figure S17 SEM image of $YbPO_4$ recovered after TGA-DSC to 1200°C.

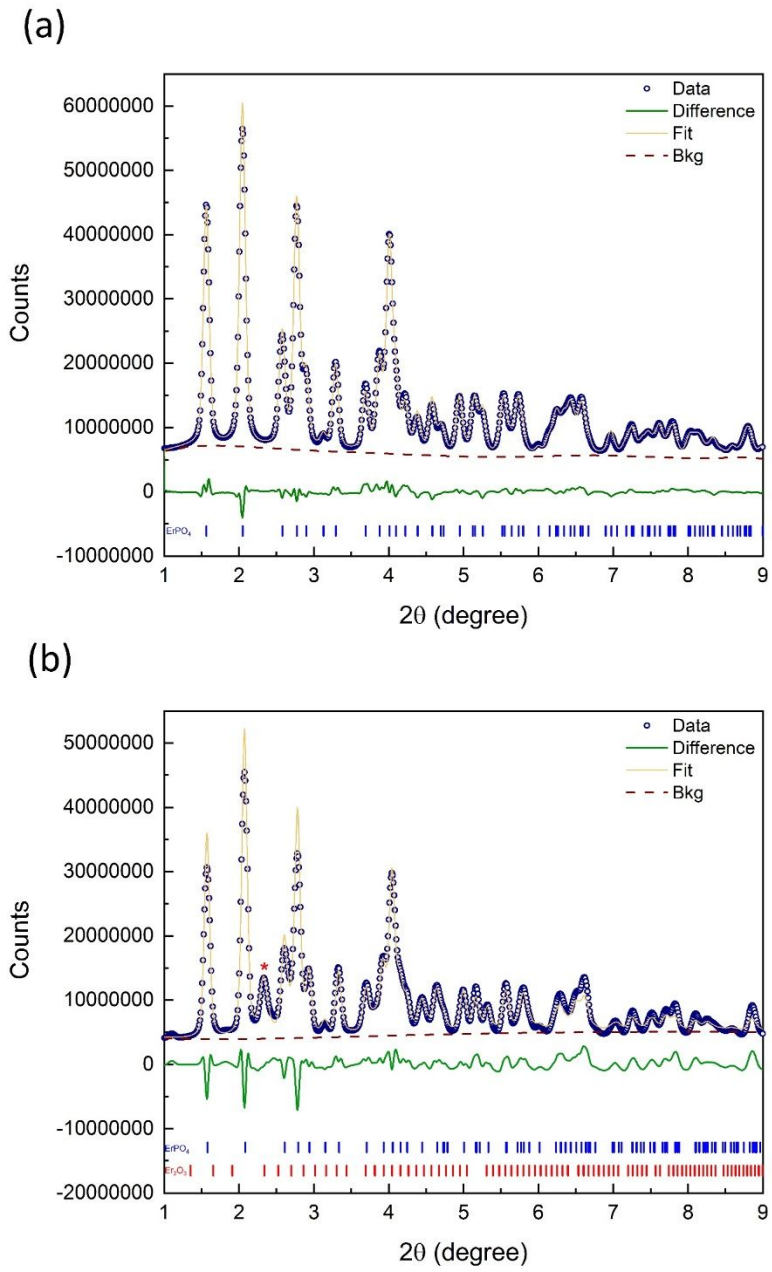

Figure S18 Representative fitted synchrotron XRD patterns from at 6 ID-D of the APS at ANL collected of the second batch of (a) pristine $ErPO_4$ and (b) $ErPO_4$ recovered after the TGA-DSC experiment to 1200°C.

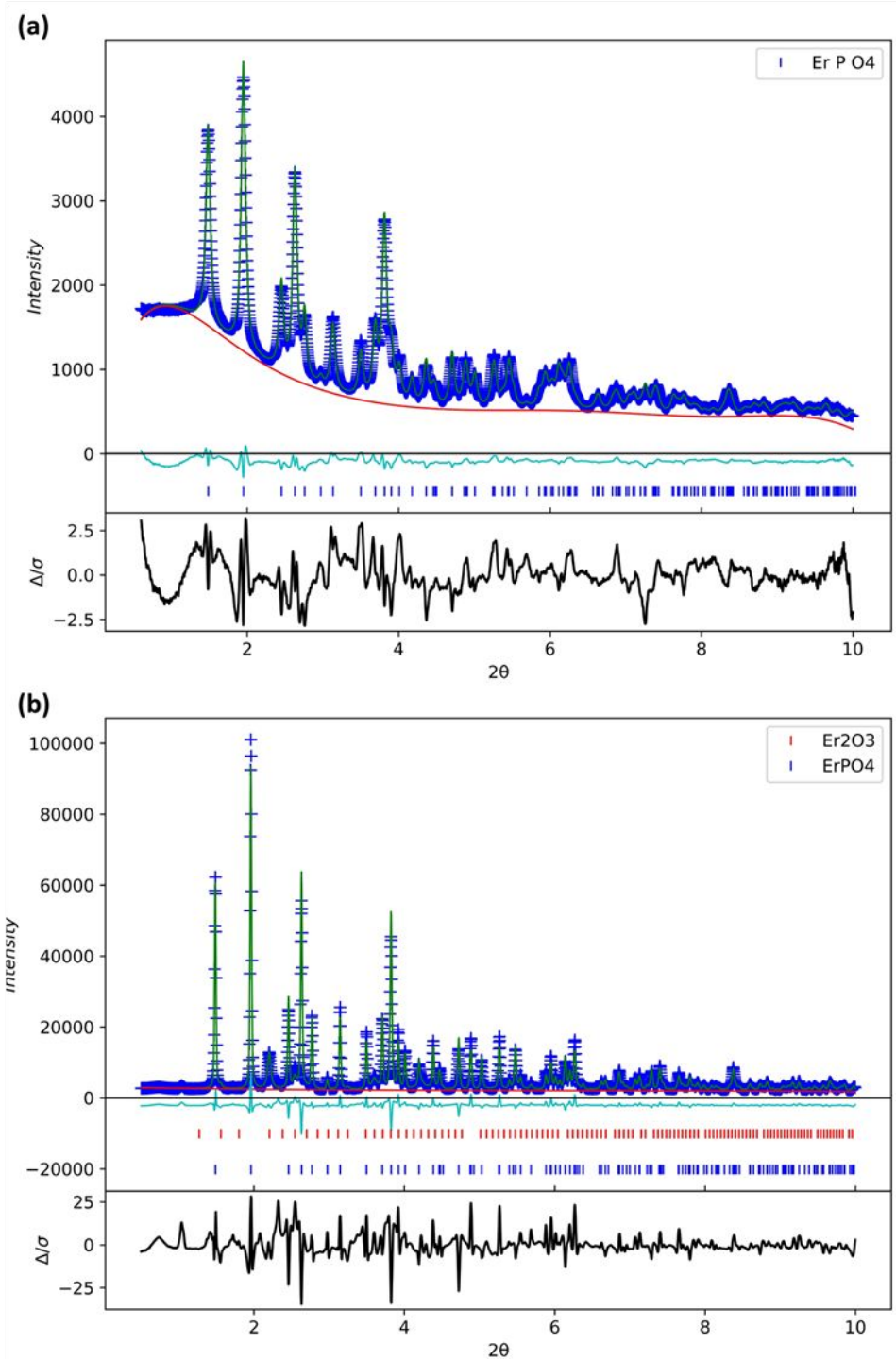

Figure S19 Representative fitted synchrotron XRD patterns from at 11 ID-C of the APS at ANL collected of the second batch of (a) pristine $ErPO_4$ and (b) $ErPO_4$ recovered after the TGA-DSC experiment to 1200°C.

Table S7 Lattice parameters, as determined by Rietveld analysis of the synchrotron powder X-ray diffraction data collected at sector 6 ID-D of the APS at ANL.

Er (x)	a-axis (Å)	c-axis (Å)	Volume (Å^3)	Rwp %	Batch #	Condition
1.0000 ± 0.0000	6.9238 ± 0.0005	5.9966 ± 0.0006	287.47 ± 0.04	3.100	1	Pristine
0.8859 ± 0.0000	6.9204 ± 0.0005	5.9952 ± 0.0005	287.12 ± 0.04	2.846	1	Pristine
0.7576 ± 0.0002	6.9032 ± 0.0005	5.9899 ± 0.0005	285.44 ± 0.04	2.677	1	Pristine
0.6343 ± 0.0002	6.8928 ± 0.0005	5.9742 ± 0.0005	283.84 ± 0.04	2.711	1	Pristine
0.4945 ± 0.0001	6.8881 ± 0.0006	5.9705 ± 0.0006	283.28 ± 0.05	2.984	1	Pristine
0.3640 ± 0.0001	6.8763 ± 0.0005	5.9666 ± 0.0006	282.13 ± 0.04	2.743	1	Pristine
0.2340 ± 0.0002	6.8693 ± 0.0006	5.9572 ± 0.0007	281.11 ± 0.05	2.900	1	Pristine
0.0000 ± 0.0000	6.8623 ± 0.0006	5.9526 ± 0.0006	280.31 ± 0.05	2.648	1	Pristine
1.0000 ± 0.0000	6.9147 ± 0.0047	6.0136 ± 0.0058	287.53 ± 0.42	3.019	2	Pristine
0.8787 ± 0.0001	6.8949 ± 0.0011	6.0072 ± 0.0013	285.58 ± 0.10	5.340	2	Pristine
0.7465 ± 0.0001	6.8978 ± 0.0013	5.9976 ± 0.0015	285.36 ± 0.11	4.813	2	Pristine
0.6175 ± 0.0002	6.8882 ± 0.0004	5.9806 ± 0.0004	283.76 ± 0.04	3.197	2	Pristine
0.4693 ± 0.0004	6.8815 ± 0.0005	5.9799 ± 0.0005	283.18 ± 0.04	3.454	2	Pristine
0.3507 ± 0.0002	6.8820 ± 0.0055	5.9627 ± 0.0061	282.41 ± 0.46	3.695	2	Pristine
0.2208 ± 0.0002	6.8567 ± 0.0005	5.9634 ± 0.0005	280.37 ± 0.04	2.977	2	Pristine
1.0000 ± 0.0000	6.8531 ± 0.0013	6.0116 ± 0.0015	282.33 ± 0.11	8.337	2	Calcinated
0.8787 ± 0.0001	6.8483 ± 0.0007	6.0022 ± 0.0008	281.50 ± 0.06	5.349	2	Calcinated
0.7465 ± 0.0001	6.8401 ± 0.0007	5.9937 ± 0.0008	280.42 ± 0.06	5.389	2	Calcinated
0.6175 ± 0.0002	6.8395 ± 0.0005	5.9918 ± 0.0006	280.29 ± 0.04	4.397	2	Calcinated
0.4693 ± 0.0004	6.8286 ± 0.0004	5.9823 ± 0.0005	278.96 ± 0.04	3.570	2	Calcinated
0.2208 ± 0.0002	6.8178 ± 0.0008	5.9752 ± 0.0009	277.74 ± 0.07	5.495	2	Calcinated
0.0000 ± 0.0000	6.8077 ± 0.0007	5.9631 ± 0.0008	276.36 ± 0.06	4.966	2	Calcinated

Table S8 Lattice parameters, as determined by Rietveld analysis of the synchrotron powder X-ray diffraction data collected at sector 11 ID-C of the APS at ANL.

Er (x)	a-axis (Å)	c-axis (Å)	Volume (Å^3)	Rwp %	Batch #	Condition
1.0000 ± 0.0000	6.9120 ± 0.0004	6.0171 ± 0.0004	287.466 ± 0.029	2.9340	2	Pristine
0.8787 ± 0.0001	6.8963 ± 0.0003	6.0048 ± 0.0003	285.583 ± 0.023	4.0720	2	Pristine
0.7465 ± 0.0001	6.8990 ± 0.0002	5.9967 ± 0.0003	285.424 ± 0.018	4.311	2	Pristine
0.6175 ± 0.0002	6.8885 ± 0.0001	5.9796 ± 0.0001	283.742 ± 0.009	5.029	2	Pristine
0.4693 ± 0.0004	6.8823 ± 0.0001	5.9785 ± 0.0001	283.177 ± 0.009	4.51	2	Pristine
0.3507 ± 0.0002	6.8825 ± 0.0002	5.9744 ± 0.0002	283.002 ± 0.013	3.676	2	Pristine
0.2208 ± 0.0002	6.8601 ± 0.0002	5.9635 ± 0.0002	280.649 ± 0.014	4.176	2	Pristine
1.0000 ± 0.0000	6.8510 ± 0.0002	6.0004 ± 0.0002	281.632 ± 0.012	8.001	2	Calcinated
0.8787 ± 0.0001	6.8502 ± 0.0001	5.9994 ± 0.0002	281.526 ± 0.010	6.915	2	Calcinated
0.7465 ± 0.0001	6.8448 ± 0.0001	5.9934 ± 0.0001	280.797 ± 0.007	5.973	2	Calcinated
0.6175 ± 0.0002	6.8402 ± 0.0001	5.9910 ± 0.0001	280.313 ± 0.007	5.121	2	Calcinated
0.4693 ± 0.0004	6.8293 ± 0.0001	5.9816 ± 0.0001	278.975 ± 0.007	4.982	2	Calcinated
0.2208 ± 0.0002	6.8193 ± 0.0002	5.9739 ± 0.0002	277.806 ± 0.012	7.465	2	Calcinated
0.0000 ± 0.0000	6.8112 ± 0.0001	5.9683 ± 0.0002	276.886 ± 0.010	5.055	2	Calcinated

Table S9 RE_2O_3 impurity as identified by synchrotron XRD.

Er [apfu]	Weight fraction RE_2O_3 Impurity	RE_2O_3 normalized mols.
1.0000	0.125 ± 0.005	0.098
0.8787	0.094 ± 0.003	0.071
0.7465	0.138 ± 0.003	0.109
0.6175	0.097 ± 0.003	0.074
0.4693	0.095 ± 0.003	0.071
0.2208	0.143 ± 0.003	0.113
0.0000	0.101 ± 0.003	0.076

Table S10 Enthalpies of Drop Solution of $Er_{(x)}Yb_{(1-x)}PO_4$ from Binary Oxides and Elements.

Formula	$\Delta H_{ds,\ uncorrected}$ (kJ/mol)	$\Delta H_{ds,\ corrected}$ (kJ/mol)
$ErPO_4$	137.08[a] ± 4.30[b] (5)[c]	147.42 ± 4.37
$Er_{0.88}Yb_{0.22}PO_4$	138.03 ± 4.94 (6)	145.48 ± 4.99
$Er_{0.75}Yb_{0.25}PO_4$	132.04± 2.25 (5)	143.36 ± 2.42
$Er_{0.62}Yb_{0.38}PO_4$	134.57 ± 3.80 (6)	142.13 ± 3.88
$Er_{0.47}Yb_{0.53}PO_4$	133.99 ± 4.39 (7)	141.25 ± 4.45
$Er_{0.22}Yb_{0.78}P$	131.30 ± 2.33 (5)	142.64 ± 2.55
$YbPO_4$	138.17 ± 2.78 (6)	145.67 ± 2.91

[a] Average. [b] Two standard deviations of the average value. [c] Number of measurements.

Table S11 Thermochemical cycles used for calculations of the enthalpy of formation from binary oxides and the standard enthalpy of formation of $Er_{(x)}Yb_{(1-x)}PO_4$ based on the data of drop solution calorimetry in molten sodium molybdate at 700°C.

Reaction	ΔH (kJ/mol)
(1) $Er_{(x)}Yb_{(1-x)}PO_{4(s,\ 25°C)} + y(Er_{(2x)}Yb_{(2-2x)}O_3)_{(s,\ 25°C)} \rightarrow [0.5+y](Er_{(2x)}Yb_{(2-2x)}O_3)_{(sln,\ 700°C)} + 0.5P_2O_{5(sln,\ 700°C)}$	$\Delta H_1 = \Delta H_{ds,\ uncorrected}$[a,b]
(2) $Er_{(x)}Yb_{(1-x)}PO_{4(s,\ 25°C)} \rightarrow 0.5(Er_{(2x)}Yb_{(2-2x)}O_3) + 0.5P_2O_{5(sln,\ 700°C)}$	$\Delta H_2 = \Delta H_{ds,\ corrected}$[a,b]
(3) $Er_2O_{3(s,\ 25°C)} \rightarrow Er_2O_{3(sln,\ 700°C)}$	ΔH_3 = -105.26[c] ± 2.48[d] (10)[e, ref1]
(4) $Yb_2O_{3(s,\ 25°C)} \rightarrow Yb_2O_{3(sln,\ 700°C)}$	ΔH_4 = -98.46 ± 3.20 (12) [ref1]
(5) $P_2O_{5(s,\ 25°C)} \rightarrow P_2O_{5(sln,\ 700°C)}$	ΔH_5 = -164.60 ± 0.85 (12) [ref1]
(6) $2Er_{(s,\ 25°C)} + 1.5O_{2(g,\ 25°C)} \rightarrow Er_2O_{3(s,\ 25°C)}$	ΔH_6 = -1900.1 ± 6.5 [ref2]
(7) $2Yb_{(s,\ 25°C)} + 1.5O_{2(g,\ 25°C)} \rightarrow Yb_2O_{3(s,\ 25°C)}$	ΔH_7 = -1814.5 ± 6.0 [ref2]
(8) $2P_{(s,\ 25°C)} + 2.5O_{2(g,\ 25°C)} \rightarrow P_2O_{5(s,\ 25°C)}$	ΔH_8 = -1504.9 ± 0.5 [ref3]

Corrected enthalpy of drop solution assuming $Er_{(2x)}Yb_{(2-2x)}O_3$ mixes as an ideal mixture:

$$\Delta H_2 = \Delta H_1 - (x \cdot y \cdot \Delta H_3) - ((1-x) \cdot y \cdot \Delta H_4)$$

Enthalpy of Mixing of $Er_{(x)}Yb_{(1-x)}PO_4$ from $ErPO_4$ and $YbPO_4$ solution:

$$\Delta H_{mix}(Er_{(x)}Yb_{(1-x)}PO_4) = -\Delta H_2 + x\Delta H_{ds}(ErPO_4) + (1-x)\Delta H_{ds}(YbPO_4)$$

Enthalpy of formation of $Er_{(x)}Yb_{(1-x)}PO_4$ from Er_2O_3, Er_2O_3, and P_2O_5

$$\Delta H_{f,\,ox}(Er_{(x)}Yb_{(1-x)}PO_4) = -\Delta H_2 + 0.5(x)\Delta H_3 + 0.5(1-x)\Delta H_4 + 0.5\Delta H_5$$

Standard enthalpy of formation of $Er_{(x)}Yb_{(1-x)}PO_4$

$$\Delta H_f(Er_{(x)}Yb_{(1-x)}PO_4) = \Delta H_{f,\,ox} + 0.5(x)\Delta H_6 + 0.5(1-x)\Delta H_7 + 0.5\Delta H_8$$

[a] Values of ΔH_1 and ΔH_2 are reported in table 1. [b] values of x and y are tabulated in table S1 and S4. [c] Average. [d] Two standard deviations of the average. [e] Number of measurements.

Ref 1 Ushakov, S. V.; Helean, K. B.; Navrotsky, A.; Boatner, L. A. Thermochemistry of Rare-Earth Orthophosphates. *J. Mater. Res.* **2001**, *16* (9), 2623–2633.

Ref 2: Konings, R. J. M.; Beneš, O.; Kovács, A.; Manara, D.; Sedmidubskỳ, D.; Gorokhov, L.; Iorish, V. S.; Yungman, V.; Shenyavskaya, E.; Osina, E. The Thermodynamic Properties of the F-Elements and Their Compounds: Part 2. The Lanthanide and Actinide Oxides. *J. Phys. Chem. Ref. Data* **2014**, *43* (1).

Ref 3: Robie, Richard A.;Hemingway, B. S. Thermodynamic Properties of Minerals and Related Substances at 298.15 K and 1 Bar (105 Pascals) Pressure and at Higher Temperatures. *U.S. Geol. Surv. Bull.* **1995**, *2131*

Table S12 Raman position of synthetic and natural xenotimes.

Chemistry of A Site	Avg. Ionic Radii of A Site	v_1 (A_{1g}) [cm^{-1}]	v_3 (B_{2g}) [cm^{-1}]	Reference
Y	1.019	1001	1058	[41]
Tb	1.040	995	1049	[41]
Dy	1.027	998	1054	[41]
Ho	1.015	1001	1055	[41]
Er	1.004	1004	1061	[41]
Tm	0.994	1006	1064	[41]
Yb	0.985	1009	1068	[41]
Lu	0.977	1011	1069	[41]
Gd	1.053	984	1046	[42]
Y	1.019	1001	1058	[43]
Sc	0.870	1027	1083	[43]
Tb	1.040	995	1049	[44]
Tb	1.040	996	1051	[44]
$Gd_{0.6}Dy_{0.4}$	1.043	995	1051	[44]
$Gd_{0.5}Dy_{0.5}$	1.040	999	1054	[44]
$Gd_{0.4}Dy_{0.6}$	1.037	996	1053	[44]

Dy	1.027	998	1054	[44]
Y	1.019	995	1049	[45]
Er	1.004	1000	1062	[45]
Tm	0.994	1006	1062	[45]
Er	1.004	1006	1063	This Study
$Er_{0.88}Yb_{0.12}$	1.002	1007	1064	This Study
$Er_{0.75}Yb_{0.25}$	0.999	1007	1065	This Study
$Er_{0.62}Yb_{0.35}$	0.997	1008	1065	This Study
$Er_{0.47}Yb_{0.35}$	0.994	1009	1067	This Study
$Er_{0.22}Yb_{0.78}$	0.989	1010	1068	This Study
Yb	0.985	1011	1070	This Study
Er	1.004	1002	1062	This Study
$Er_{0.88}Yb_{0.12}$	1.002	1003	1063	This Study
$Er_{0.75}Yb_{0.25}$	0.999	1001	1063	This Study
$Er_{0.62}Yb_{0.35}$	0.997	1002	1064	This Study
$Er_{0.47}Yb_{0.35}$	0.994	1002	1065	This Study
$Er_{0.35}Yb_{0.65}$	0.992	1002	1065	This Study
$Er_{0.22}Yb_{0.78}$	0.989	1004	1067	This Study
Yb	0.985	1005	1067	This Study
$Y_{0.65}Dy_{0.08}Er_{0.06}Yb_{0.06}U_{0.03}Lu_{0.03}Gd_{0.02}Ho_{0.02}Th_{0.01}Tm_{0.01}Tb_{0.01}Sm_{0.01}$	1.017	999	1057	[46]
$Y_{0.64}Dy_{0.08}Er_{0.08}Yb_{0.08}Lu_{0.03}Gd_{0.03}Ho_{0.02}U_{0.02}Tm_{0.01}Tb_{0.01}Sm_{0.01}Nd_{0.01}$	1.016	997		[46]
$Y_{0.61}Ca_{0.11}Dy_{0.04}Th_{0.04}Yb_{0.03}Er_{0.03}Zr_{0.03}Gd_{0.02}U_{0.02}Fe_{0.02}Sm_{0.01}Ho_{0.01}Tm_{0.01}Nd_{0.01}Tb_{0.01}$	1.018	992	1057	[47]
$Y_{0.72}Dy_{0.05}U_{0.04}Yb_{0.04}Er_{0.03}Zr_{0.03}Th_{0.03}Gd_{0.02}Sm_{0.01}Ho_{0.01}Nd_{0.01}Lu_{0.01}Tb_{0.01}Tm_{0.01}$	1.015	993	1057	[47]
$Y_{0.74}Dy_{0.05}Yb_{0.04}Er_{0.04}Zr_{0.03}Gd_{0.02}U_{0.02}Th_{0.01}Sm_{0.01}Ho_{0.01}Tm_{0.01}Tb_{0.01}Lu_{0.01}Nd_{0.01}$	1.013	994	1056	[47]
$Y_{0.79}Dy_{0.05}Er_{0.04}Yb_{0.01}Gd_{0.03}Sm_{0.01}Ho_{0.01}Tm_{0.01}Lu_{0.01}U_{0.01}Nd_{0.01}Tb_{0.01}$	1.019	995	1053	[47]
$Y_{0.74}Dy_{0.09}Gd_{0.06}Er_{0.04}Yb_{0.02}Ho_{0.01}Tb_{0.01}Sm_{0.01}Eu_{0.01}$	1.022	998	1056	[48]
$Y_{0.85}Dy_{0.11}Yb_{0.04}$	1.019	999	1056	[49]

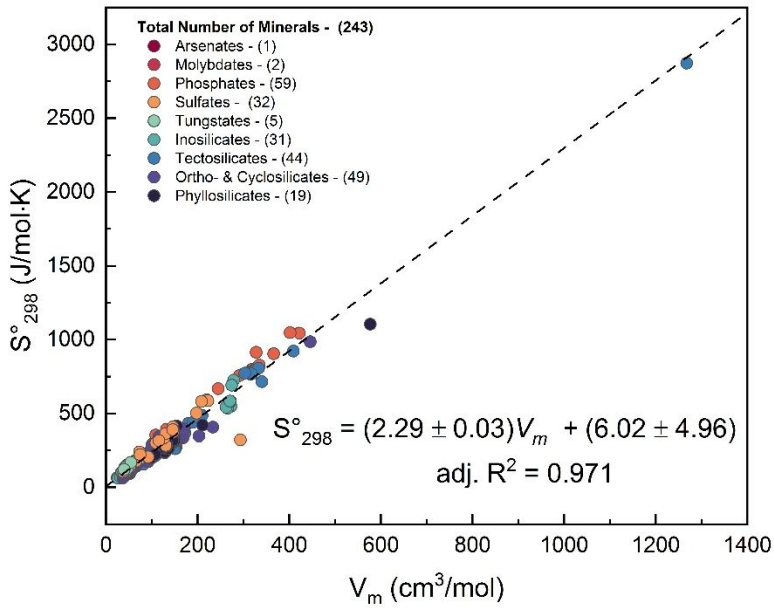

Figure S20 Empirical model for determining S° from V_m for all minerals. References for all phases is reported in Table S7.

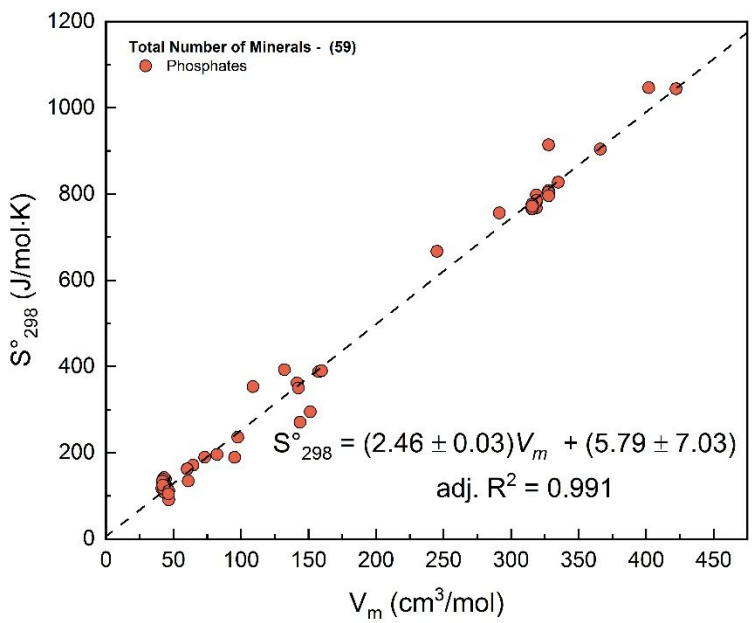

Figure S21 Empirical model for determining S° from V_m for phosphate minerals. References for all phases is reported in Table S7.

Table S13 Molar Volume and Standard Entropy Data used in Figures S3 and S4 used in Empirical model for determining S° from V_m for phosphate minerals.

Name	Chemistry	Anion	V_m (cm^3)	$S°_{298}$ (J/mol·K)	Ref $S°_{298}$	Ref. V_m
olivenite	$Cu_2(AsO_4)(OH)$	AsO_4	63.7131	179.5	16	16
powellite	$CaMoO_4$	MoO_4	47	122.6	17	17
wulfenite	$PbMoO_4$	MoO_4	53.86	166.1	17	17
berlinite	$AlPO_4$	PO_4	46.58	90.8	17	17
whitlockite	$Ca_3(PO4)_2$	PO_4	97.62	236	17	17
fluoroapatite	$Ca_5(PO4)_3F$	PO_4	157.56	387.9	17	17
hydroxyapatite	$Ca_5(PO4)_3OH$	PO_4	159.6	390.4	17	17
strengite	$FePO_4·2H_2O$	PO_4	64.5	171.3	17	17
xenotime-(Tb)	$TbPO_4$	PO_4	44.08	138.1	18	19
xenotime-(Dy)	$DyPO_4$	PO_4	43.57	116.6	18	19
xenotime-(Ho)	$HoPO_4$	PO_4	43.07	142.3	18	19
xenotime-(Er)	$ErPO_4$	PO_4	42.6	116.6	18	19
xenotime-(Tm)	$TmPO_4$	PO_4	42.2	138.1	18	19
xenotime-(Yb)	$YbPO_4$	PO_4	41.78	133.9	18	19
xenotime-(Lu)	$LuPO_4$	PO_4	41.43	117.2	18	19
xenotime-(Y)	YPO_4	PO_4	42.96	108.8	18	19
monazite-(La)	$LaPO_4$	PO_4	46.02	108.3	18	19
monazite-(Ce)	$CePO_4$	PO_4	45.27	120	18	19
monazite-(Pr)	$PrPO_4$	PO_4	44.65	123.2	18	19
monazite-(Nd)	$NdPO_4$	PO_4	43.99	122.9	18	19
monazite-(Sm)	$SmPO_4$	PO_4	43	122.5	18	19
monazite-(Eu)	$EuPO_4$	PO_4	42.49	117.2	18	19
monazite-(Gd)	$GdPO_4$	PO_4	42.15	124.6	18	19
farringtonite	$Mg_3(PO4)_2$	PO_4	95.37	189.2	20	21
moneite	CaHPO4	PO_4	46.58	111.4	20	22
brushite	CaHPO4·2H2O	PO_4	73.15	189.45	20	23
variscite	$AlPO_4·2H_2O$	PO_4	60.98	134.5	20	24

gallium orthophosphate	$GaPO_4$	PO_4	46.19	105	[20]	[25]
lead phosphate	$Pb_3(PO4)_2$	PO_4	108.84	353.34	[20]	[26]
minyulite	$KAI_2(PO_4)_2(OH)\cdot 2H_2O$	PO_4	151.26	294.68	[20]	[27]
trolleite	$Al_4(OH)_3[PO_4]_3$	PO_4	143.72	270.7	[20]	[28]
fluorapatite	$Ca_{10}(PO_4)_6F_2$	PO_4	315.6	775.7	[20]	[29]
hydroxylapatite	$Ca_{10}(PO_4)_6(OH)_2$	PO_4	318.75	780.7	[20]	[29]
chloroapatite	$Ca_{10}(PO_4)_6Cl_2$	PO_4	327.8	795.8	[20]	[30]
hydroxylapatite	$Ca_{10}(PO_4)_6(OH)_2$	PO_4	318.75	768	[31]	[29]
hydroxylapatite	$Ca_{10}(PO_4)_6(OH)_2$	PO_4	318.75	781.1	[31]	[29]
hydroxylapatite	$Ca_{10}(PO_4)_6(OH)_2$	PO_4	318.75	780.8	[31]	[29]
hydroxylapatite	$Ca_{10}(PO_4)_6(OH)_2$	PO_4	318.75	797.9	[31]	[29]
hydroxylapatite	$Ca_{10}(PO_4)_6(OH)_2$	PO_4	318.75	785	[31]	[29]
fluorapatite	$Ca_{10}(PO_4)_6F_2$	PO_4	315.6	765	[31]	[29]
fluorapatite	$Ca_{10}(PO_4)_6F_2$	PO_4	315.6	776.5	[31]	[29]
fluorapatite	$Ca_{10}(PO_4)_6F_2$	PO_4	315.6	775.8	[31]	[29]
fluorapatite	$Ca_{10}(PO_4)_6F_2$	PO_4	315.6	766.4	[31]	[29]
fluorapatite	$Ca_{10}(PO_4)_6F_2$	PO_4	315.6	771.8	[31]	[29]
chloroapatite	$Ca_{10}(PO_4)_6Cl_2$	PO_4	327.8	914	[31]	[30]
chloroapatite	$Ca_{10}(PO_4)_6Cl_2$	PO_4	327.8	800.2	[31]	[30]
chloroapatite	$Ca_{10}(PO_4)_6Cl_2$	PO_4	327.8	801.2	[31]	[30]
chloroapatite	$Ca_{10}(PO_4)_6Cl_2$	PO_4	327.8	808	[31]	[30]
chloroapatite	$Ca_{10}(PO_4)_6Cl_2$	PO_4	327.8	804.3	[31]	[30]
chloroapatite	$Ca_{10}(PO_4)_6Cl_2$	PO_4	327.8	796.2	[31]	[30]
barium chlorapatite	$Ba_{10}(PO_4)_6Cl_2$	PO_4	422.15	1044	[31]	[32]
strontium chlorapatite	$Sr_{10}(PO_4)_6Cl_2$	PO_4	366.17	904	[31]	[33]
bromoapatite	$Ca_{10}(PO_4)_6Br_2$	PO_4	334.97	827.3	[31]	[34]
saleeite	$Mg(UO_2)_2(PO_4)_2\cdot 10(H_2O)$	PO_4	291.37	756	[35]	[36]
meta-autunite	$Ca(UO_2)_2(PO_4)_2\cdot 6(H_2O)$	PO_4	245.13	667	[35]	[37]
libethenite	$Cu_2(PO_4)(OH)$	PO_4	60.1501	162.2	[16]	[16]

pseudomalachite	$Cu_5(PO_4)_2(OH)$	PO_4	132.147	392.7	16	16
newberyite	$MgHPO_4{\cdot}3H_2O$	PO_4	82.2	195.9	38	38
phosphorrosslerite	$MgHPO_4{\cdot}7H_2O$	PO_4	141.6	361.8	38	38
k-struvite	$MgKPO_4{\cdot}6H_2O$	PO_4	142.5	350.1	38	38
farringtonite	$Mg_3(PO4)_2$	PO_4	95.2	189.2	38	38
cattiite	$Mg_3(PO_4)_2{\cdot}22H_2O$	PO_4	401.9	1046.6	38	38
wollanstonite	$CaSiO_3$	SiO_4 - C&B	39.9	81.7	17	17
pseudowollanstonite	$CaSiO_3$	SiO_4 - C&B	40.08	87.2	17	17
wollanstonite $_{glass}$	$CaSiO_3$	SiO_4 - C&B	40.13	94.8	17	17
Ca-Al pyroxene	$CaAl_2SiO_6$	SiO_4 - C&B	63.57	141	17	17
Ca-Al pyroxene $_{glass}$	$CaAl_2SiO_6$	SiO_4 - C&B	78.13	155.3	17	17
ferrobustamite	$CaFeSi_2O_6$	SiO_4 - C&B	73	180.5	17	17
hedenbergite	$CaFeSi_2O_6$	SiO_4 - C&B	67.95	174.2	17	17
hedenbergite $_{glass}$	$CaFeSi_2O_6$	SiO_4 - C&B		185.7	17	17
diopside	$CaMgSi_2O_6$	SiO_4 - C&B	66.09	142.7	17	17
diopside $_{glass}$	$CaMgSi_2O_6$	SiO_4 - C&B	76.09	166	17	17
ferrosilite	$FeSiO_3$	SiO_4 - C&B	33	94.6	17	17
α-spodumene	$LiAlSi_2O_6$	SiO_4 - C&B	58.37	129.3	17	17
β-spodumene	$LiAlSi_2O_6$	SiO_4 - C&B	78.25	154.4	17	17
enstatite	$MgSiO_3$	SiO_4 - C&B	31.31	66.3	17	17
enstatite $_{glass}$	$MgSiO_3$	SiO_4 - C&B	36.6	74.1	17	17

clinoenstatite	$MgSiO_3$	SiO_4 - C&B	31.28	67.9	17	17
$MgSiO_3$ - pervoskite	$MgSiO_3$	SiO_4 - C&B	24.5	63.6	17	17
$MgSiO_3$ - ilmenite	$MgSiO_3$	SiO_4 - C&B	26.36	60.4	17	17
hypersthene	$(Mg_{0.85}Fe_{0.15})SiO_3$	SiO_4 - C&B	31.53	69	17	17
rhodonite	$MnSiO_3$	SiO_4 - C&B	34.94	100.5	17	17
pyromagite	$MnSiO_3$	SiO_4 - C&B	34.72	99.4	17	17
jadeite	$NaAlSi_2O_6$	SiO_4 - C&B	60.4	133.5	17	17
jadeite $_{glass}$	$NaAlSi_2O_6$	SiO_4 - C&B		170.5	17	17
acmite	$NaFeSi_2O_6$	SiO_4 - C&B	64.6	170.6	17	17
tremolite	$Ca_2Mg_5Si_8O_{22}(OH)_2$	SiO_4 - C&B	272.9	548.9	17	17
grunerite	$Fe_7Si_8O_{22}(OH)_2$	SiO_4 - C&B	278.7	725	17	17
anthrophyllite	$Mg_7Si_8O_{22}(OH)_2$	SiO_4 - C&B	265.4	534.5	17	17
riebeckite	$NaFe_3Fe_2Si_8O_{22}(OH)_2$	SiO_4 - C&B	274.7	691	17	17
glaucophane	$Na_2Mg_3Al_2Si_8O_{22}(OH)_2$	SiO_4 - C&B	262.1	541.2	17	17
pargasite	$NaCa_2Mg_4Al(Al_2Si_6)O_{22}(OH)_2$	SiO_4 - C&B	272	582	17	17
fluoropargasite	$NaCa_2Mg_4Al(Al_2Si_6)O_{22}F_2$	SiO_4 - C&B	270.6	583	17	17
edingtonite (ordered)	$BeAl_2Si_3O_{10}\cdot 3H_2O$	SiO_4- F	180.4	434.8	17	17
anorthite	$CaAl_2Si_2O_8$	SiO_4- F	100.79	199.3	17	17
hexagonal anorthite	$CaAl_2Si_2O_8$	SiO_4- F	99.85	214.8	17	17
anorthite glass	$CaAl_2Si_2O_8$	SiO_4- F	103	237.3	17	17

stilbite	$Ca_{1.02}Na_{0.14}K_{0.01}(Al_{2.18}Si_{6.82}O_{18})\cdot 7.33H_2O$	SiO_4- F	333.4	805.9	17	17
heulandite	$Ca_{0.59}Sr_{0.18}Ba_{0.06}Na_{0.38}K_{0.13}Al_{2.16}Si_{6.84}O_{18}\cdot 6H_2O$	SiO_4- F	317.6	767.2	17	17
wairakite	$CaAl_2Si_4O_{12}\cdot 2H_2O$	SiO_4- F	190.4	440	17	17
laumontite	$CaAl_2Si_4O_{12}\cdot 4H_2O$	SiO_4- F	211.3		17	17
scolecite	$CaAl_2Si_3O_{10}\cdot 3H_2O$	SiO_4- F	172.3	367.4	17	17
leonhardite	$Ca_2Al_4Si_8O_{24}\cdot 7H_2O$	SiO_4- F	409.3	922.2	17	17
bicchulite	$Ca_2Al_2SiO_6(OH)_2$	SiO_4- F	103.68	213.1	17	17
meionite (Al/Si ordered)	$Ca_4Al_6Si_6O_{24}CO_3$	SiO_4- F	340.36	715.2	17	17
danburite	$CaB_2Si_2O_8$	SiO_4- F	82.2	155.3	17	17
clinoptilolite	$(Na_{0.56}K_{0.98}Ca_{1.50}Mg_{1.23})(Al_{6.7}Fe_{0.3})Si_{29}O_{72}\cdot 22H_2O$	SiO_4- F	1267.6	2872.3	17	17
pollucite	$(Cs_{0.65}Na_{0.19}Rb_{0.03})Al_2Si_4O_{12}\cdot H_2O$	SiO_4- F	83	207.2	17	17
mircocline	$KAlSi_3O_8$	SiO_4- F	108.72	214.2	17	17
sanidine	$KAlSi_3O_8$	SiO_4- F	109.05	232.8	17	17
K-feldspar glass	$KAlSi_3O_8$	SiO_4- F	116.5	261.6	17	17
kaliophillite	$KAlSiO_4$	SiO_4- F	59.89	133.3	17	17
leucite	$KAlSi_2O_6$	SiO_4- F	88.27	200.2	17	17
eucryptite	$LiAlSiO_4$	SiO_4- F	53.63	103.8	17	17
petalite	$LiAlSi_4O_{10}$	SiO_4- F	128.4	233.2	17	17
albite	$NaAlSi_3O_8$	SiO_4- F	100.07	207.4	17	17
analbite	$NaAlSi_3O_8$	SiO_4- F	100.43	225.6	17	17
albite $_{glass}$	$NaAlSi_3O_8$	SiO_4- F	110.1	251.9	17	17
Na-K feldspar ss.	$Na_{0.85}K_{0.15}AlSi_3O_8$	SiO_4- F	102.18	231.3	17	17
Na-K feldspar ss.	$Na_{0.55}K_{0.45}AlSi_3O_8$	SiO_4- F	105.22	237	17	17
na-k feldspar ss.	$Na_{0.25}K_{0.75}AlSi_3O_8$	SiO_4- F	107.37	237.4	17	17
nepheline	$NaAlSiO_4$	SiO_4- F	54.19	124.4	17	17
carnegieite	$NaAlSiO_4$	SiO_4- F	56.03	118.7	17	17
nepheline $_{glass}$	$NaAlSiO_4$	SiO_4- F	56.86	134.5	17	17
analcime	$NaAlSi_2O_6\cdot H_2O$	SiO_4- F	97.4	227.7	17	17
dehydrated analcime	$NaAlSi_2O_6$	SiO_4- F		172.5	17	17

natrolite	$Na_2Al_2Si_3O_{10}\cdot 2H_2O$	SiO_4- F	169.2	359.7	[17]	[17]
phillpsite	$(Na_{1.1}K_{0.8})Al_{1.9}Si_{6.1}O_{16}\cdot 6H_2O$	SiO_4- F	303	771.9	[17]	[17]
mesolite	$Na_{0.68}Ca_{0.66}(Al_{1.99}Si_{3.01}O_{10})\cdot 2.65H_2O$	SiO_4- F	171.1	363	[17]	[17]
mordenite	$Na_{0.36}Ca_{0.29}Al_{0.94}Si_{5.06}O_{12}\cdot 3.47H_2O$	SiO_4- F	209.8	486.5	[17]	[17]
dehydrated mordenite	$Na_{0.36}Ca_{0.29}Al_{0.94}Si_{5.06}O_{12}$	SiO_4- F		299.1	[17]	[17]
merlinoite	$Na_{0.81}K_{0.19}AlSi_{1.94}O_{5.88}\cdot 2.13H_2O$	SiO_4- F	150.6	282.4	[17]	[17]
merlinoite	$K_{0.80}Na_{0.20}AlSi_{1.94}O_{5.88}\cdot 1.88H_2O$	SiO_4- F	152.2	276.6	[17]	[17]
merlinoite	$KAlSi_{1.94}O_{5.88}\cdot 1.69H_2O$	SiO_4- F	151.2	274.3	[17]	[17]
merlinoite	$K_{0.81}Na_{0.19}AlSi_{1.81}O_{5.62}\cdot 2.18H_2O$	SiO_4- F	153.6	274.6	[17]	[17]
merlinoite	$K_{0.91}Na_{0.09}AlSi_{1.81}O_{5.62}\cdot 1.79H_2O$	SiO_4- F	151.5	260.5	[17]	[17]
merlinoite	$KAlSi_{1.81}O_{5.62}\cdot 1.69H_2O$	SiO_4- F	149.8	259.7	[17]	[17]
topaz	$Al_2SiO_4F_2$	SiO_4- O&R	51.53	105.4	[17]	[17]
kyanite	Al_2SiO_5	SiO_4- O&R	44.15	82.8	[17]	[17]
andalusite	Al_2SiO_5	SiO_4- O&R	51.52	91.4	[17]	[17]
sillmanite	Al_2SiO_5	SiO_4- O&R	49.86	95.4	[17]	[17]
mullite	$Al_6Si_2O_{13}$	SiO_4- O&R	134.55	275	[17]	[17]
dumortierite	$Al_{6.75}0_{0.25}Si_2BO_{17.25}(OH)_{0.75}$	SiO_4- O&R	168.4	334.9	[17]	[17]
euclase	$BeAlSiO_4(OH)$	SiO_4- O&R	46.86	89.1	[17]	[17]
phenakite	Be_2SiO_4	SiO_4- O&R	37.18	63.4	[17]	[17]
beryl	$Be_3Al_2(Si_6O_{18})$	SiO_4- O&R	203.3	346.7	[17]	[17]
bertrandite	$Be_4Si_2O_7(OH)_2$	SiO_4- O&R	91.8	172.1	[17]	[17]
epidote	$Ca_2Al_2FeSi_3O_{12}(OH)$	SiO_4- O&R	138.1	328.9	[17]	[17]
lawsonite	$Ca_2Al_2[Si_2O_7(OH)_2]H_2O$	SiO_4- O&R	101.32	230	[17]	[17]

gehlenite	$CaAl_2SiO_7$	SiO_4-O&R	90.15	210	[17]	[17]
zoisite	$Ca_2Al_3Si_3O_{12}(OH)$	SiO_4-O&R	136.5	295.9	[17]	[17]
grossular	$Ca_3Al_2Si_3O_{12}$	SiO_4-O&R	125.28	260.1	[17]	[17]
grossular$_{(glass)}$	$Ca_3Al_2Si_3O_{12}$	SiO_4-O&R	158.8	329.2	[17]	[17]
datolite	$CaB(SiO_4)(OH)$	SiO_4-O&R	53.32	110.2	[17]	[17]
ilvaite	$CaFe_2Fe(Si_2O_7)O(OH)$	SiO_4-O&R	101.07	292.3	[17]	[17]
andradite	$Ca_3Fe_2Si_3O_{12}$	SiO_4-O&R	132.04	316.4	[17]	[17]
monticellite	$CaMgSiO_4$	SiO_4-O&R	51.3	108.1	[17]	[17]
akermanite	$Ca_2MgSi_2O_7$	SiO_4-O&R	92.54	212.5	[17]	[17]
merwinite	$Ca_3Mg(SiO_4)_2$	SiO_4-O&R	98.5	253.1	[17]	[17]
titanite	$CaTiSiO_5$	SiO_4-O&R	55.74	129.2	[17]	[17]
larnite	α-Ca_2SiO_4	SiO_4-O&R	51.6	127.6	[17]	[17]
calcio-olivine	γ-Ca_2SiO_4	SiO_4-O&R	58.01	120.5	[17]	[17]
haturite	Ca_3SiO_5	SiO_4-O&R	72.74	168.6	[17]	[17]
rankinite	$Ca_3Si_2O_7$	SiO_4-O&R	96.51	210.6	[17]	[17]
rosenhahnite	$Ca_3Si_3O_8(OH)_2$	SiO_4-O&R	126.46	281.8	[17]	[17]
spurrite	$Ca_5(SiO_4)_2CO_3$	SiO_4-O&R	146.97	331	[17]	[17]
tilleyite	$Ca_5Si_2O_7(CO_3)_2$	SiO_4-O&R	170.5	394	[17]	[17]
cobalt-olivine	Co_2SiO_4	SiO_4-O&R	44.49	142.6	[17]	[17]

fayalite	Fe_2SiO_4	SiO_4-O&R	46.31	151	[17]	[17]
almandine	$Fe_3Al_2Si_3O_{12}$	SiO_4-O&R	115.32	342.6	[17]	[17]
staurolite	$Fe_4Al_{18}Si_8O_{46}(OH)_2$	SiO_4-O&R	445.9	985	[17]	[17]
osumilite	$KMg_2Al_3[Si_{10}Al_2O_{30}]\cdot H_2O$	SiO_4-O&R	379.2		[17]	[17]
cordierite	$Mg_2Al_3(AlSi_5O_{18})$	SiO_4-O&R	233.22	407.2	[17]	[17]
sapphirine	$Mg_2Al_4O_6(SiO_4)$	SiO_4-O&R	98.9	197.5	[17]	[17]
forsterite	Mg_2SiO_4	SiO_4-O&R	43.65	94.1	[17]	[17]
pyrope	$Mg_3Al_2Si_3O_{12}$	SiO_4-O&R	113.12	266.3	[17]	[17]
$pyrope_{glass}$	$Mg_3Al_2Si_3O_{12}$	SiO_4-O&R	146.1	346.3	[17]	[17]
pyrope-grossular ss.	$(Mg_{1.8}Ca_{1.2})Al_2Si_3O_{12}$	SiO_4-O&R	118.35	268.3	[17]	[17]
pyrope-grossular $ss._{glass}$	$(Mg_{1.5}Ca_{1.5})Al_2Si_3O_{12}$	SiO_4-O&R	152.5	311.8	[17]	[17]
tephroite	Mn_2SiO_4	SiO_4-O&R	48.99	155.9	[17]	[17]
liebenbergite	Ni_2SiO_4	SiO_4-O&R	42.57	128.1	[17]	[17]
nickel spinel	Ni_2SiO_4	SiO_4-O&R	39.81	124.1	[17]	[17]
willmenite	Zn_2SiO_4	SiO_4-O&R	52.42	131.4	[17]	[17]
zircon	$ZrSiO_4$	SiO_4-O&R	39.26	84	[17]	[17]
coffinite	$USiO_4$	SiO_4-O&R	45.99	136	[39]	[39]
thorite	$ThSiO_4$	SiO_4-O&R	48.61	147.05	[40]	[40]
dickite	$Al_2Si_2O_5(OH)_4$	SiO_4- S	98.56	197.1	[17]	[17]
kaolinite	$Al_2Si_2O_5(OH)_4$	SiO_4- S	99.34	200.4	[17]	[17]

halloysite	$Al_2Si_2O_5(OH)_4$	SiO_4- S		203	17	17
pyrophyllite	$Al_2Si_4O_{10}(OH)_2$	SiO_4- S	128.1	239.4	17	17
illite	$K_3(Al_7Mg)(Al_2Si_{14})O_{40}(OH)_8$	SiO_4- S	577	1104.2	17	17
margarite	$CaAl_2[Al_2Si_2O_{10}](OH)_2$	SiO_4- S	129.63	263.6	17	17
prehnite	$CaAl_2[AlSi_3O_{10}](OH)_2$	SiO_4- S	141.1	292.8	17	17
muscovite (al/si disordered)	$KAl_2[Al_2Si_3O_{10}](OH)_2$	SiO_4- S	140.81	306.4	17	17
muscovite (al/si ordered)	$KAl_2[Al_2Si_3O_{10}](OH)_2$	SiO_4- S	140.81	287.7	17	17
annite	$KFe_3[Al_2Si_3O_{10}](OH)_2$	SiO_4- S	154.3	415	17	17
phlogopite (Al/Si disordered)	$KMg_3[Al_2Si_3O_{10}](OH)_2$	SiO_4- S	149.65	334.6	17	17
phlogopite (Al/Si disordered)	$KMg_3[Al_2Si_3O_{10}](OH)_2$	SiO_4- S	149.65	315.9	17	17
fluorphlogopite (Al/Si disordered)	$KMg_3[Al_2Si_3O_{10}]F_2$	SiO_4- S	146.52	336.3	17	17
fluorphlogopite (Al/Si disordered)	$KMg_3[Al_2Si_3O_{10}]F_2$	SiO_4- S	146.52	317.6	17	17
talc	$Mg_3Si_4O_{10}(OH)_2$	SiO_4- S	136.2	260.8	17	17
chrysotile	$Mg_3Si_2O_5(OH)_4$	SiO_4- S	107.5	221.3	17	17
clinochlore	$Mg_5Al(AlSi_3O_{10})(OH)_8$	SiO_4- S	211	421	17	17
paragonite (Al/Si disordered)	$NaAl_2(AlSi_3O_{10})(OH)_2$	SiO_4- S	132.1	295.8	17	17
paragonite (al/si ordered)	$NaAl_2(AlSi_3O_{10})(OH)_2$	SiO_4- S	132.1	277.1	17	17
aluminum sulfate	$Al_2(SO_4)_3$	SO_4	73.41	239.3	17	17
barite	$BaSO_4$	SO_4	52.1	132.2	17	17
anhydrite	$CaSO_4$	SO_4	46.01	107.4	17	17
gypsum	$CaSO_4 \cdot 2H_2O$	SO_4	74.69	193.8	17	17
chalcocyanite	$CuSO_4$	SO_4	40.88	109.5	17	17
chalcanthite	$CuSO_4 \cdot 5H_2O$	SO_4	108.97	301.2	17	17
brochanthite	$Cu_4(SO_4)(OH)_6$	SO_4			17	17
ferric sulfate	$Fe_2(SO_4)_3$	SO_4	130.8	282.8	17	17
szomolnokite	$FeSO_4 \cdot H_2O$	SO_4			17	17

melanterite	$FeSO_4 \cdot 7H_2O$	SO_4	146.5	409.2	[17]	[17]
arcanite	K_2SO_4	SO_4	65.5	175.6	[17]	[17]
k-al sulfate	$KAl(SO_4)_2$	SO_4	92.33	204.6	[17]	[17]
alunite	$KAl_3(OH)_6(SO_4)_2$	SO_4	293.6	321	[17]	[17]
langbeinite	$KMg_3(SO_4)_3$	SO_4	146.95	389.3	[17]	[17]
magnesium sulfate	$MgSO_4$	SO_4			[17]	[17]
epsomite	$MgSO_4 \cdot 7H_2O$	SO_4	146.8	372	[17]	[17]
manganese sulfate	$MnSO_4$	SO_4	43.62	127	[17]	[17]
mascagnite	$(NH_4)_2SO_4$	SO_4	74.68	220.5	[17]	[17]
thenardite	Na_2SO_4	SO_4	53.33	149.6	[17]	[17]
mirabilite	$Na_2SO_4 \cdot 10H_2O$	SO_4	219.8	591.9	[17]	[17]
nickelous sulfate	$NiSO_4$	SO_4	38.57	101.3	[17]	[17]
retersite	$NiSO_4 \cdot 6H_2O$	SO_4	126.6	334.5	[17]	[17]
morenosite	$NiSO_4 \cdot 7H_2O$	SO_4	143.8	378.9	[17]	[17]
anglesite	$PbSO_4$	SO_4	47.95	148.5	[17]	[17]
celestite	$SrSO_4$	SO_4	46.25	117	[17]	[17]
zinokiste	$ZnSO_4$	SO_4	41.57	110.5	[17]	[17]
bianchite	$ZnSO_4 \cdot 6H_2O$	SO_4	130.2	363.6	[17]	[17]
goslarite	$ZnSO_4 \cdot 7H_2O$	SO_4	145.8	388.7	[17]	[17]
borax	$Na_2B_4O_7 \cdot 10H_2O$	SO_4	222.7	586	[17]	[17]
kröhnkite	$Na_2Cu(SO_4) \cdot 2H_2O$	SO_4	115.79	315.5	[16]	[16]
cyanochroite	$K_2Cu(SO_4)_2 \cdot 6H_2O$	SO_4	197.84	501.9	[16]	[16]
devilline	$CaCu_4(SO_4)_2(OH)_6 \cdot 3H_2O$	SO_4	208.708	581.2	[16]	[16]
scheelite	$CaWO_4$	WO_4	47.05	126.4	[17]	[17]
ferberite	$FeWO_4$	WO_4	40.38	131.8	[17]	[17]
huebnerite	$MnWO_4$	WO_4	41.89	132.5	[17]	[17]
stolzite	$PbWO_4$	WO_4	54.1	168.2	[17]	[17]
sanmartinite	$ZnWO_4$	WO_4	39.79	119.3	[17]	[17]

Table S14 Thermodynamic functions derived for $ErPO_4$-$YbPO_4$ solid solution, ΔH_{mix} is that determined by empirical volumetric method.

Er (*x*)	ΔH_{mix} (kJ/mol)	ΔH_f (kJ/mol)	$S°$ (J/mol·K)	$\Delta S_{mix, vib}$ (J/mol·K)	$\Delta S_{mix, config}$ (J/mol·K)	$\Delta S_{mix, total}$ (J/mol·K)	ΔS_f (J/mol·K)
1.0000	0.00	-1976.9	110.2	0.0	0.0	0.0	-415.7
0.8787	0.05	-1971.1	110.1	0.1	3.1	3.1	-411.0
0.7465	0.08	-1964.8	109.7	0.0	4.7	4.7	-407.8
0.6175	0.10	-1958.6	109.6	0.1	5.5	5.7	-405.1
0.4693	0.11	-1951.6	109.1	-0.1	5.7	5.7	-403.4
0.2208	0.07	-1939.8	108.7	0.0	4.4	4.4	-401.5
0.0000	0.00	-1929.4	108.2	0.0	0.0	0.0	-403.1

Table S15 Free Energy of Mixing for $ErPO_4$-$YbPO_4$ solid solution at various temperatures, using volumetrically determined ΔH_{mix}

	ΔG_{mix} (kJ/mol)			
Er(x)	T = 25°C	T = 100°C	T = 250°C	T = 400°C
1.0000	0	0	0	0
0.8787	-0.89	-2.06	-3.70	-5.81
0.7465	-1.32	-3.07	-5.53	-8.70
0.6175	-1.59	-3.70	-6.67	-10.48
0.4693	-1.59	-3.71	-6.68	-10.50
0.2208	-1.23	-2.86	-5.15	-8.10
0.0000	0	0	0	0

Table S16 Free Energy of Mixing for $ErPO_4$-$YbPO_4$ solid solution at various temperatures, using experimentally calorimetry determined ΔH_{mix}

	ΔG_{mix} (kJ/mol)			
Er(x)	T = 25°C	T = 100°C	T = 250°C	T = 400°C
1.0000	0	0	0	0
0.8787	0.79	-0.38	-2.03	-4.14
0.7465	2.22	0.46	-2.00	-5.16
0.6175	2.93	0.81	-2.15	-5.97
0.4693	3.55	1.43	-1.54	-5.37
0.2208	2.12	0.48	-1.81	-4.75
0.0000	0	0	0	0

Table S17 $C_p = a + bT + cT^2$, derived from Neumann-Koop's rule. T = Temperature in K

Er (x)	a			b			c			Adj. R^2
1.0000	55.976	±	1.99177	0.19692	±	0.00704	-7.77E-05	±	5.53E-06	0.99907
0.8787	56.5624	±	1.98058	0.19628	±	0.007	-7.75E-05	±	5.50E-06	0.99907
0.7465	57.20166	±	1.96839	0.19558	±	0.00696	-7.73E-05	±	5.46E-06	0.99907
0.6175	57.82575	±	1.95649	0.19489	±	0.00692	-7.71E-05	±	5.43E-06	0.99907
0.4693	58.54229	±	1.94282	0.19411	±	0.00687	-7.69E-05	±	5.39E-06	0.99908
0.2208	59.74369	±	1.91991	0.19279	±	0.00679	-7.65E-05	±	5.33E-06	0.99909
0.0000	60.81157	±	1.89954	0.19163	±	0.00671	-7.62E-05	±	5.27E-06	0.99909

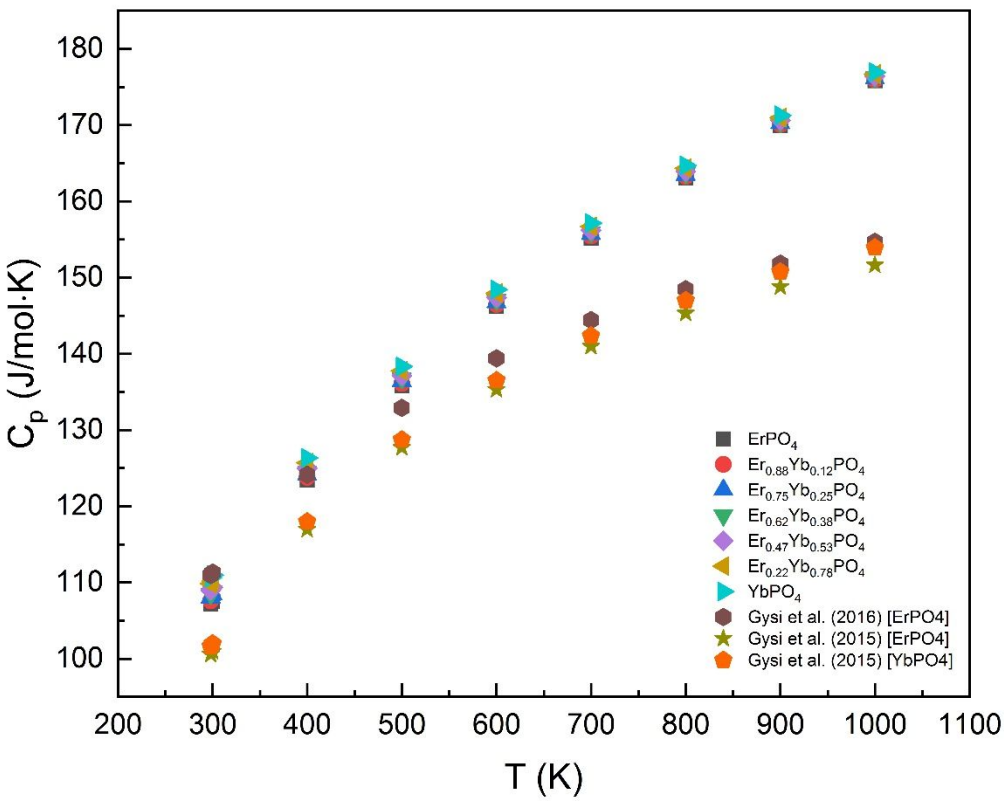

Figure S22 Comparison of the C_p derived by NKR versus those reported in the literature that were derived experimentally.

Table S18 Results from the integration of C_p equation from Table S11.

	$\int_{298}^{T} C_p dT$ [kJ/mol]						
T [°C]	$ErPO_4$	$Er_{0.88}Yb_{0.12}PO_4$	$Er_{0.75}Yb_{0.25}PO_4$	$Er_{0.62}Yb_{0.38}PO_4$	$Er_{0.47}Yb_{0.53}PO_4$	$Er_{0.22}Yb_{0.78}PO_4$	$YbPO_4$
25	0.00	0.00	0.00	0.00	0.00	0.00	0.00
27	0.22	0.22	0.22	0.22	0.22	0.22	0.22
127	11.75	11.79	11.83	11.87	11.92	12.00	12.07
227	24.63	24.70	24.78	24.86	24.94	25.09	25.23
327	38.70	38.80	38.91	39.02	39.14	39.35	39.54
427	53.80	53.93	54.07	54.20	54.36	54.62	54.85
527	69.79	69.94	70.10	70.26	70.44	70.74	71.01
627	86.50	86.67	86.85	87.03	87.23	87.57	87.87
727	103.79	103.97	104.17	104.35	104.58	104.95	105.28

Table S19 $C_p/T = a + bT + cT^2$, derived from Neumann-Koop's rule. T = Temperature in K

Er (x)	a			b			c			Adj. R^2
1.0000	0.52175	±	0.00965	-6.42E-04	±	3.41E-05	2.99E-07	±	2.68E-08	0.99701
0.8787	0.52455	±	0.00982	-6.48E-04	±	3.47E-05	3.03E-07	±	2.73E-08	0.99695
0.7465	0.52762	±	0.01	-6.54E-04	±	3.53E-05	3.06E-07	±	2.78E-08	0.99688
0.6175	0.5306	±	0.01017	-6.60E-04	±	3.59E-05	3.10E-07	±	2.82E-08	0.99682
0.4693	0.53404	±	0.01037	-6.67E-04	±	3.67E-05	3.14E-07	±	2.88E-08	0.99675
0.2208	0.53979	±	0.01071	-6.79E-04	±	3.79E-05	3.20E-07	±	2.97E-08	0.99662
0.0000	0.5449	±	0.01101	-6.90E-04	±	3.89E-05	3.26E-07	±	3.06E-08	0.99652

Table S20 Results from the integration of C_p/T equation from Table S13.

	$\int_{298}^{T} \frac{C_p}{T} dT$ [kJ/mol·K]						
T [°C]	$ErPO_4$	$Er_{0.88}Yb_{0.12}PO_4$	$Er_{0.75}Yb_{0.25}PO_4$	$Er_{0.62}Yb_{0.38}PO_4$	$Er_{0.47}Yb_{0.53}PO_4$	$Er_{0.22}Yb_{0.78}PO_4$	$YbPO_4$
25	0.00	0.00	0.00	0.00	0.00	0.00	0.00
27	0.00	0.00	0.00	0.00	0.00	0.00	0.00
127	0.03	0.03	0.03	0.03	0.03	0.03	0.04
227	0.06	0.06	0.06	0.06	0.06	0.06	0.07
327	0.09	0.09	0.09	0.09	0.09	0.09	0.09
427	0.11	0.11	0.11	0.11	0.11	0.11	0.12
527	0.13	0.13	0.13	0.13	0.13	0.14	0.14
627	0.15	0.15	0.15	0.15	0.15	0.15	0.16
727	0.17	0.17	0.17	0.17	0.17	0.17	0.17

Table S21 Gibbs free energy of formation as a function of T, using volumetrically determined ΔH_{mix}.

	ΔG$_f$(kJ/mol)						
Temperature (°C)	$ErPO_4$	$Er_{0.88}Yb_{0.12}PO_4$	$Er_{0.75}Yb_{0.25}PO_4$	$Er_{0.62}Yb_{0.38}PO_4$	$Er_{0.47}Yb_{0.53}PO_4$	$Er_{0.22}Yb_{0.78}PO_4$	$YbPO_4$
25	-1853.0	-1848.6	-1843.3	-1837.9	-1831.4	-1820.2	-1809.3
27	-1852.2	-1847.8	-1842.4	-1837.1	-1830.6	-1819.4	-1808.5
127	-1812.5	-1808.6	-1803.6	-1798.5	-1792.2	-1781.2	-1770.1
227	-1776.2	-1772.8	-1768.1	-1763.3	-1757.1	-1746.4	-1735.2
327	-1742.5	-1739.6	-1735.2	-1730.7	-1724.8	-1714.2	-1703.0
427	-1711.0	-1708.5	-1704.5	-1700.4	-1694.6	-1684.3	-1672.9
527	-1681.4	-1679.5	-1675.8	-1671.9	-1666.4	-1656.3	-1644.8
627	-1653.8	-1652.4	-1649.1	-1645.5	-1640.2	-1630.4	-1618.8
727	-1628.5	-1627.6	-1624.6	-1621.4	-1616.2	-1606.7	-1595.0

Calculated through the following equation:

$$\Delta G_T = \left[\Delta H_{298} + \int_{298}^{T} C_p dT\right] - \left[T * \left(\Delta S_{298} + \int_{298}^{T} \frac{C_p}{T} dT\right)\right]$$

Table S22 Gibbs free energy of formation as a function of T, using experimentally calorimetry determined ΔH_{mix}.

	ΔG_f(kJ/mol)						
Temperature (°C)	$ErPO_4$	$Er_{0.88}Yb_{0.12}PO_4$	$Er_{0.75}Yb_{0.25}PO_4$	$Er_{0.62}Yb_{0.38}PO_4$	$Er_{0.47}Yb_{0.53}PO_4$	$Er_{0.22}Yb_{0.78}PO_4$	$YbPO_4$
25	-1860.97	-1854.84	-1847.55	-1841.19	-1833.95	-1824.42	-1816.78
27	-1860.14	-1854.02	-1846.73	-1840.37	-1833.15	-1823.61	-1815.98
127	-1820.47	-1814.84	-1807.87	-1801.8	-1794.75	-1785.42	-1777.63
227	-1784.13	-1778.99	-1772.36	-1766.58	-1759.72	-1750.62	-1742.71
327	-1750.43	-1745.78	-1739.5	-1734.01	-1727.35	-1718.49	-1710.47
427	-1718.9	-1714.75	-1708.81	-1703.63	-1697.17	-1688.55	-1680.41
527	-1689.34	-1685.69	-1680.09	-1675.21	-1668.96	-1660.58	-1652.33
627	-1661.77	-1658.62	-1653.38	-1648.8	-1642.75	-1634.61	-1626.26
727	-1636.46	-1633.82	-1628.93	-1624.66	-1618.82	-1610.95	-1602.5

Calculated through the following equation:

$$\Delta G_T = \left[\Delta H_{298} + \int_{298}^{T} C_p dT\right] - \left[T * \left(\Delta S_{298} + \int_{298}^{T} \frac{C_p}{T} dT\right)\right]$$

Reference:

(1) Mesbah, A.; Clavier, N.; Lozano-Rodriguez, M. J.; Szenknect, S.; Dacheux, N. Incorporation of Thorium in the Zircon Structure Type through the Th1-XErx(SiO4)1-x(PO4)x Thorite-Xenotime Solid Solution. *Inorg. Chem.* **2016**, *55* (21), 11273–11282. https://doi.org/10.1021/acs.inorgchem.6b01862.

(2) Bruker Nano GmbH. S2 Picofox™. Bruker Nano GmbH: Berlin 2010.

(3) Bruker Nano GmbH. Spectra 7. Bruker Nano GmbH: Berlin 2010.

(4) Lenz, C.; Nasdala, L.; Talla, D.; Hauzenberger, C.; Seitz, R.; Kolitsch, U. Laser-Induced REE3+ Photoluminescence of Selected Accessory Minerals - An "Advantageous Artefact" in Raman Spectroscopy. *Chem. Geol.* **2015**, *415* (October), 1–16. https://doi.org/10.1016/j.chemgeo.2015.09.001.

(5) Prescher, C.; Prakapenka, V. B. DIOPTAS: A Program for Reduction of Two-Dimensional X-Ray Diffraction Data and Data Exploration. *High Press. Res.* **2015**, *35* (3), 223–230. https://doi.org/10.1080/08957959.2015.1059835.

(6) Toby, B. H.; Von Dreele, R. B. GSAS-II: The Genesis of a Modern Open-Source All Purpose Crystallography Software Package. *J. Appl. Crystallogr.* **2013**, *46* (2), 544–549. https://doi.org/10.1107/S0021889813003531.

(7) Guo, X.; Szenknect, S.; Mesbah, A.; Labs, S.; Clavier, N.; Poinssot, C.; Ushakov, S. V.; Curtius, H.; Bosbach, D.; Ewing, R. C.; et al. Thermodynamics of Formation of Coffinite, USiO4. *Proc. Natl. Acad. Sci.* **2015**, *112* (21), 6551–6555. https://doi.org/10.1073/pnas.1507441112.

(8) Tavakoli, A. H.; Maram, P. S.; Widgeon, S. J.; Rufner, J.; Van Benthem, K.; Ushakov, S.; Sen, S.; Navrotsky, A. Amorphous Alumina Nanoparticles: Structure, Surface Energy, and Thermodynamic Phase Stability. *J. Phys. Chem. C* **2013**, *117* (33), 17123–17130. https://doi.org/10.1021/jp405820g.

(9) Guo, X.; Tiferet, E.; Qi, L.; Solomon, J. M.; Lanzirotti, A.; Newville, M.; Engelhard, M. H.; Kukkadapu, R. K.; Wu, D.; Ilton, E. S.; et al. U(v) in Metal Uranates: A Combined Experimental and Theoretical Study of MgUO4, CrUO4, and FeUO4. *Dalt. Trans.* **2016**, *45* (11), 4622–4632. https://doi.org/10.1039/c6dt00066e.

(10) Guo, X.; Wu, D.; Xu, H.; Burns, P. C.; Navrotsky, A. Thermodynamic Studies of Studtite Thermal Decomposition Pathways via Amorphous Intermediates UO3, U2O7, and UO4. *J. Nucl. Mater.* **2016**, *478*, 158–163. https://doi.org/10.1016/j.jnucmat.2016.06.014.

(11) Navrotsky, A. Progress and New Directions in Calorimetry: A 2014 Perspective. *J. Am. Ceram. Soc.* **2014**, *97* (11), 3349–3359. https://doi.org/10.1111/jace.13278.

(12) Strzelecki, A. C.; Ren, Y.; Chong, S.; Riley, B. J.; Xu, H.; McCloy, J. S.; Guo, X. Structure and Thermodynamics of Calcium Rare Earth Silicate Oxyapatites, Ca2RE8(SiO4)6O2 (RE = Pr, Tb, Ho, Tm). *Phys. Chem. Miner.* **2021**, *Pending Re*.

(13) Strzelecki, A. C.; Kriegsman, K. W.; Estevenon, P.; Goncharov, V.; Bai, J.; Szenknect, S.; Mesbah, A.; Wu, D.; McCloy, J. S.; Dacheux, N.; et al. High-Temperature Thermodynamics of Cerium Silicates, A-Ce2Si2O7 and Ce4.67(SiO4)3O. *ACS Earth Sp. Chem.* **2020**, *4* (11), 2129–2143. https://doi.org/10.1021/acsearthspacechem.0c0023.

(14) Strzelecki, A. C.; Bourgeois, C.; Kriegsman, K. W.; Estevenon, P.; Wei, N.; Szenknect, S.; Mesbah, A.; Wu, D.; Ewing, R. C.; Dacheux, N.; et al. Thermodynamics of CeSiO4 : Implications for Actinide Orthosilicates. *Inorg. Chem.* **2020**, *59* (18), 13174–13183. https://doi.org/10.1021/acs.inorgchem.0c01476.

(15) Zhang, X.; Reece, M. E.; Cockreham, C. B.; Sun, H.; Wang, B.; Xu, H.; Sun, J.; Guo, X.; Su, H.; Wang, Y.; et al. Formation Energetics and Guest—Host Interactions of Molybdenum Carbide Confined in Zeolite Y. *Ind. Eng. Chem. Res.* **2021**. https://doi.org/10.1021/acs.iecr.1c02822.

(16) Majzlan, J.; Zittlau, A. H.; Grevel, K. D.; Schliesser, J.; Woodfield, B. F.; Dachs, E.; Števko, M.; Chovan, M.; Plášil, J.; Sejkora, J.; et al. Thermodynamic Properties and Phase Equilibria of the Secondary Copper Minerals Libethenite, Olivenite, Pseudomalachite, Kröhnkite, Cyanochroite, and Devilline. *Can. Mineral.* **2016**, *53* (5), 937–960. https://doi.org/10.3749/canmin.1400066.

(17) Robie, Richard A.;Hemingway, B. S. Thermodynamic Properties of Minerals and Related Substances at 298.15 K and 1 Bar (105 Pascals) Pressure and at Higher Temperatures. *U.S. Geol. Surv. Bull.* **1995**, *2131*.

(18) Navrotsky, A.; Lee, W.; Mielewczyk-Gryn, A.; Ushakov, S. V.; Anderko, A.; Wu, H.; Riman, R. E. Thermodynamics of Solid Phases Containing Rare Earth Oxides. *J. Chem. Thermodyn.* **2015**, *88*, 126–141. https://doi.org/10.1016/j.jct.2015.04.008.

(19) Ushakov, S. V.; Helean, K. B.; Navrotsky, A.; Boatner, L. A. Thermochemistry of Rare-Earth Orthophosphates. *J. Mater. Res.* **2001**, *16* (9), 2623–2633. https://doi.org/10.1557/JMR.2001.0361.

(20) Vieillard, P.; Tardy, Y. Thermochemical Properties of Phosphates. *Phosphate Miner.* **1984**, 171–198. https://doi.org/10.1007/978-3-642-61736-2_4.

(21) Nord, A. G.; Kierkegaard, P. The Crystal Structure of Mg3(PO4)2. *Acta Chem. Scand. A* **1968**, *22*, 1466–1474.

(22) Catti, M.; Ferraris, G.; Filhol, A. Hydrogen Bonding in the Crystalline State. CaHPO4 (Monetite), P1 or P1? A Novel Neutron Diffraction Study. *Acta Crystallogr. Sect. B Struct. Crystallogr. Cryst. Chem.* **1977**, *33* (4), 1223–1229. https://doi.org/10.1107/s0567740877005706.

(23) Schofield, P. F.; Knight, K. S.; van der Houwen, J. A. M.; Valsami-Jones, E. The Role of Hydrogen Bonding in the Thermal Expansion and Dehydration of Brushite, Di-Calcium Phosphate Dihydrate. *Phys. Chem. Miner.* **2004**, *31* (9), 606–624. https://doi.org/10.1007/s00269-004-0419-6.

(24) Kniep, R.; Mootz, D.; Vegas, A. Variscite. *Acta Crystallogr. Sect. B Struct. Crystallogr. Cryst. Chem.* **1977**, *33* (1), 263–265. https://doi.org/10.1107/s056774087700329x.

(25) Gorfman, S.; Tsirelson, V.; Pucher, A.; Morgenroth, W.; Pietsch, U. X-Ray Diffraction by a Crystal in a Permanent External Electric Field: Electric-Field-Induced Structural Response in α-GaPO4. *Acta Crystallogr. Sect. A Found. Crystallogr.* **2006**, *62* (1), 1–10. https://doi.org/10.1107/S0108767305036111.

(26) Angel, R. J.; Bismayer, U.; Marsha, W. G. Renormalization of the Phase Transition in Lead Phosphate, Pb3(PO4)2, by High Pressure: Structure. *J. Phys. Condens. Matter* **2001**, *13* (22), 5353–5364. https://doi.org/10.1088/0953-8984/13/22/325.

(27) Kampf, A. R. Minyulite : Its Atomic Arrangement. *Am. Mineral.* **1977**, *62*, 256–262.

(28) Moore, P. B.; Araki, T. Trolleite, Al4(OH)3[PO4]3: A Very Dense Structure with Octahedral Face-Sharing Dimers. *Am. Mineral.* **1974**, *59*, 974–984.

(29) Bulina, N. V.; Makarova, S. V.; Prosanov, I. Y.; Vinokurova, O. B.; Lyakhov, N. Z. Structure and Thermal Stability of Fluorhydroxyapatite and Fluorapatite Obtained by Mechanochemical Method. *J. Solid State Chem.* **2020**, *282* (July 2019), 121076. https://doi.org/10.1016/j.jssc.2019.121076.

(30) Fang, Y. N.; Ritter, C.; White, T. J. Crystal Chemical Characteristics of Ellestadite-Type Apatite: Implications for Toxic Metal Immobilization. *Dalt. Trans.* **2014**, *43* (42), 16031–16043. https://doi.org/10.1039/c4dt02088j.

(31) Drouet, C. A Comprehensive Guide to Experimental and Predicted Thermodynamic Properties of Phosphate Apatite Minerals in View of Applicative Purposes. *J. Chem. Thermodyn.* **2015**, *81*, 143–159. https://doi.org/10.1016/j.jct.2014.09.012.

(32) Hata, M.; Marumo, F.; Iwai, S.; Aoki, H. Structure of Barium Chlorapatite. *Acta Crystallogr. Sect. B Struct. Crystallogr. Cryst. Chem.* **1979**, *35* (10), 2382–2384. https://doi.org/10.1107/s0567740879009377.

(33) Chen, J.; Liang, Y.; Zhu, Y.; Liu, S.; Li, H.; Lei, W. Abnormal Reduction of Eu3+ to Eu2+ in Sr5(PO4)3Cl:Eu Phosphor and Its Enhanced Red Emission by the Charge Compensation. *J. Lumin.* **2019**, *214* (May), 116569. https://doi.org/10.1016/j.jlumin.2019.116569.

(34) Elliott, J. C.; Dykes, E.; Mackie, P. E. Structure of Bromapatite and the Radius of the Bromide Ion. *Acta Crystallogr. Sect. B Struct. Crystallogr. Cryst. Chem.* **1981**, *37* (2), 435–438. https://doi.org/10.1107/s0567740881003208.

(35) Suleimanov, E. V.; Chernorukov, N. G.; Veridusova, V. V.; Nipruk, O. V. Physical Chemistry of Barium Uranophosphate and Uranoarsenate. *Radiochemistry* **2006**, *48* (2), 155–158. https://doi.org/10.1134/S1066362206020093.

(36) Miller, S. A. Mg[U02P04]2. **1986**, *253*, 247–253.

(37) Makarov, E. S.; Ivanov, V. I. The Crystal Structure of Meta-Autunite Ca(UO2)2(PO4)2*6H2O. *Dokl. Acad. Sci. USSR, Earth Sci. Sect.* **1960**, *132*, 601–603.

(38) Lothenbach, B.; Xu, B.; Winnefeld, F. Thermodynamic Data for Magnesium (Potassium) Phosphates. *Appl. Geochemistry* **2019**, *111* (May), 104450. https://doi.org/10.1016/j.apgeochem.2019.104450.

(39) Szenknect, S.; Mesbah, A.; Cordara, T.; Clavier, N.; Brau, H. P.; Le Goff, X.; Poinssot, C.; Ewing, R. C.; Dacheux, N. First Experimental Determination of the Solubility Constant of Coffinite. *Geochim. Cosmochim. Acta* **2016**, *181*, 36–53. https://doi.org/10.1016/j.gca.2016.02.010.

(40) Szenknect, S.; Costin, D. T.; Clavier, N.; Mesbah, A.; Poinssot, C.; Vitorge, P.; Dacheux, N. From Uranothorites to Coffinite: A Solid Solution Route to the Thermodynamic Properties of USiO4. *Inorg. Chem.* **2013**, *52* (12), 6957–6968. https://doi.org/10.1021/ic400272s.

(41) Begun, G. M.; Beall, G. W.; Boatner, L. A.; Gregor, W. J. Raman Spectra of the Rare Earth Orthophosphates. *J. Raman Spectrosc.* **1982**, *11* (4), 273–278. https://doi.org/10.1002/jrs.1250130315.

(42) Clavier, N.; Mesbah, A.; Szenknect, S.; Dacheux, N. Monazite, Rhabdophane, Xenotime & Churchite: Vibrational Spectroscopy of Gadolinium Phosphate Polymorphs. *Spectrochim. Acta - Part A Mol. Biomol. Spectrosc.* **2018**, *205*, 85–94. https://doi.org/10.1016/j.saa.2018.07.016.

(43) Giarola, M.; Sanson, A.; Rahman, A.; Mariotto, G.; Bettinelli, M.; Speghini, A.; Cazzanelli, E. Vibrational Dynamics of YPO4 and ScPO4 Single Crystals: An Integrated Study by Polarized Raman Spectroscopy and First-Principles Calculations. *Phys. Rev. B - Condens. Matter Mater. Phys.* **2011**, *83* (22), 1–8. https://doi.org/10.1103/PhysRevB.83.224302.

(44) Musselman, M. A.; Wilkinson, T. M.; Haberl, B.; Packard, C. E. In Situ Raman Spectroscopy of Pressure-Induced Phase Transformations in Polycrystalline TbPO4, DyPO4, and GdxDy(1−x)PO4. *J. Am. Ceram. Soc.* **2018**, *101* (6), 2562–2570. https://doi.org/10.1111/jace.15374.

(45) Stavrou, E.; Tatsi, A.; Salpea, E.; Boulmetis, Y. C.; Kontos, A. G.; Raptis, Y. S.; Raptis, C. Raman Study of Zircon-Structured RPO4 (R = Y, Tb, Er, Tm) Phosphates at High Pressures. *J. Phys. Conf. Ser.* **2008**, *121* (PART 4). https://doi.org/10.1088/1742-6596/121/4/042016.

(46) Maftei, A. E.; Buzatu, A.; Damian, G.; Buzgar, N.; Dill, H. G.; Apopei, A. I. Micro-Raman — A Tool for the Heavy Mineral Deposits, Gold Placer-Type (Valley, Pianu). *Minerals* **2020**, *10* (988), 1–17. https://doi.org/doi:10.3390/min10110988.

(47) Švecová, E.; Čopjaková, R.; Losos, Z.; Škoda, R.; Nasdala, L.; Cícha, J. Multi-Stage Evolution of Xenotime–(Y) from Písek Pegmatites, Czech Republic: An Electron Probe Micro-Analysis and Raman Spectroscopy Study. *Mineral. Petrol.* **2016**, *110* (6), 747–765. https://doi.org/10.1007/s00710-016-0442-6.

(48) Origlieri, M. Xenotime-(Y) R050178 https://rruff.info/Xenotime-(Y)/R050178 (accessed Oct 12, 2021).

(49) Obodda, H. Xenotime-(Y) R060428 https://rruff.info/xenotime/display=default/R060428 (accessed Oct 12, 2021).